Fermilab

New Technologies for Axion and Dark Photon Searches

FERMILAB-PUB-24-0933-T

arXiv:2412.08704

New Technologies for Axion and Dark Photon Searches

Asher Berlin[1,2], Yonatan Kahn[2,3,4]

[1]Theoretical Physics Division, Fermi National Accelerator Laboratory, Batavia, IL 60510, USA; email: aberlin@fnal.gov
[2]Superconducting Quantum Materials and Systems Center (SQMS), Fermi National Accelerator Laboratory, Batavia, IL 60510, USA
[3]Illinois Center for Advanced Studies of the Universe and Department of Physics, University of Illinois Urbana-Champaign, Urbana, IL 61801, USA
[4] Department of Physics, University of Toronto, Toronto, ON M5S 1A7, Canada; email: yf.kahn@utoronto.ca

Abstract

The search for dark matter and physics beyond the Standard Model has grown to encompass a highly interdisciplinary approach. In this review, we survey recent searches for light, weakly-coupled particles – axions and dark photons – over the past decade, focusing on new experimental results and the incorporation of technologies and techniques from fields as diverse as quantum science, microwave engineering, precision magnetometry, and condensed matter physics. We also review theoretical progress which has been useful in identifying new experimental directions, and identify the areas of most rapid experimental progress and the technological advances required to continue exploring the parameter space for axions and dark photons.

Contents

1. Introduction

Near the turn of the 21st century, compelling signatures predicted by weak-scale supersymmetric theories fueled the anticipation of new discoveries at upcoming experiments, such as the Large Hadron Collider and the next generation of underground dark matter direct detection experiments (1, 2, 3). As a result, much of the activity in the field of high-energy physics was driven by a small set of common paradigms for what might lie beyond the Standard Model. Today, although it is certainly possible that the ongoing operation of such experiments might soon discover new physics near the electroweak ($\sim$ TeV) scale, it may be the case that the majority of their discovery potential has already been exhausted.

This state of affairs has led to a considerable relaxation in the community's priors for where new physics might first be unveiled (4). For instance, although it would be theoretically appealing if dark matter were found to be related to other fundamental problems of the Standard Model such as the hierarchy problem, there is no first-principles reason for such a connection. It is also possible that new physics at high energies is well beyond the reach of even the most powerful future colliders. However, even if this were true, dynamics at extremely high energies can give rise to new feebly-coupled low-energy degrees of freedom, motivating observational signatures that are accessible to small-scale *precision* experiments. Two examples of such hypothetical particles, and the focus of this review, are the "axion" and "dark photon," i.e., dark sector analogs of the ordinary pion and photon that are ubiquitous in theories involving extra dimensions and gauge-coupling unification (5, 6, 7).

Driven by these shifts in priors and the thirst for data, many high-energy physicists, theorists and experimentalists alike, have become deeply involved in conceiving and developing small-scale probes for low-energy signatures of new physics (8, 9). These endeavors span a plethora of different subfields involving connections between condensed matter physics, atomic physics, and quantum information science. Compared to two decades ago, the high-energy physics community therefore finds itself in a healthy state of increased diversification.

In this review, we aim to provide a useful entry point for non-experts interested in laboratory precision probes of ultralight axions and dark photons. In the past twenty years, there have been multiple articles of this type (see, e.g., Refs. (10, 11)), which have surveyed then-current developments of the most well-known experimental approaches, such as cav-

ity haloscopes, helioscopes, and light-shining-through-wall experiments. Since then, these experiments have improved both their sensitivity and overall scope, but the past decade has also seen an explosion of completely new experimental ideas. Two major developments leveraged by several of these experiments are quantum sensing technology (including squeezed vacuum states and non-demolition measurements such as single-photon counting) and the maturation of high-Q superconducting radiofrequency (SRF) cavities, originally designed for accelerator applications and now harnessed in the search for new physics.

An additional goal of this review is to provide an update on the impressive experimental progress within this diverse field, as well as to identify recent changes in the community's theory priors. Despite this progress, there still remain large gaps in coverage, i.e., regions of theory space that will not be covered by any current proposal. We therefore hope to motivate young theorists and experimentalists to seek the new ideas required to tackle these elusive regions of model space. As we aim to provide a high-level overview, we focus more on experimental concepts than technical details, and refer the reader to the references provided for further study.

The next section begins with a more-detailed overview of the theoretical motivations, priors, and target regions of parameter space for the models considered here. The remaining sections will then discuss laboratory-based searches for ultralight axions and dark photons, depending on whether they do or do not constitute the dark matter of our galaxy. While we unfortunately do not have space in this review to cover the plethora of astrophysical or cosmological probes of axions and dark photons, we refer the reader to the excellent compendia in Refs. (12, 13, 14, 15). Throughout, we use a mostly-negative spacetime metric $(+, -, -, -)$ and natural units wherein $\hbar = c = k_B = 1$.

2. Theory

2.1. Motivation

As mentioned above, axions and dark photons can be motivated by top-down considerations such as extra dimensions and gauge-coupling unification, but they are phenomenologically important because these particles can also explain the dark matter of our universe. In this section, we discuss such bottom-up perspectives, as well as outline the various ways in which axions and dark photons couple to Standard Model fields.

Although the observational evidence for dark matter is overwhelming, direct evidence of its particle properties is almost negligible. However, much can still be learned from basic astrophysical observations and simple theoretical requirements. Taking dark matter to be described by a Poincaré-invariant quantum field theory, it is either a boson or fermion. Then, quantum mechanics can be applied on galactic scales to place a lower bound on the dark matter mass m_{DM} by demanding that dark matter dominated objects, such as dwarf galaxies, are gravitationally stable. In the case of fermionic dark matter, the Pauli exclusion principle implies that the Fermi velocity does not exceed the gravitational escape velocity of such systems for $m_{\mathrm{DM}} \gtrsim 100$ eV (16). Therefore, sub-eV dark matter must be bosonic. A lower bound on the mass of bosonic dark matter can be derived from the Heisenberg uncertainty principle, which imposes a minimum velocity dispersion for spatially-confined particles. For a galaxy to host a bosonic dark matter halo, the dark matter de Broglie wavelength must be smaller than the size of the galaxy, yielding the constraint $m_{\mathrm{DM}} \gtrsim 10^{-21}$ eV $- 10^{-19}$ eV (17, 18). To proceed further, the interactions of ultralight bosons with spin ≥ 2 are severely restricted by Lorentz covariance (19, 20, 21, 22).

As a result, we are motivated to consider exclusively spin-0 (scalar) or spin-1 (vector) bosons, which are much less constrained and lead to a larger variety of potential signals.

A massive vector field A'^μ with couplings $A'_\mu J^\mu$ to conserved Standard Model currents J^μ is a well-behaved quantum-mechanical theory; by analogy with the vector field of electromagnetism, we refer to such a field as a dark photon. The situation is not as simple for spin-0 particles. A new spin-0 scalar boson that is invariant under the combination of parity and time-reversal symmetry would have a hierarchy problem even more severe than the Higgs, with quantum threshold corrections from couplings to any heavy particles tending to push its mass up to the highest possible scale (see, e.g., Ref. (23) for a recent review). On the other hand, a parity-odd pseudoscalar field "a" may be naturally light if it originates as a pseudo-Goldstone boson of a global U(1) symmetry spontaneously-broken at a scale f_a, analogous to the pion of QCD. We will refer to such particles as axions throughout the review, reserving the term "QCD axion" for a scenario where the spontaneously-broken symmetry is a "Peccei-Quinn symmetry" responsible for solving the strong-CP problem (24). This origin for the axion field imposes strong requirements on the structure of its couplings to Standard Model fields, providing an appealing target for direct detection experiments aiming to probe axion interactions with photons, nucleons, and electrons.

With the motivational underpinnings of axions and dark photons in place, we can now enumerate their interactions with Standard Model fields. Since the axion is a pseudo-Goldstone boson generated by the breaking of a new global U(1) symmetry, its mass and interactions arise analogously to those of the Standard Model pion, such that $m_a \sim \Lambda_a^2/f_a$ (for the QCD axion, Λ_a is roughly the QCD scale $\Lambda_{\rm QCD}$). The axion's couplings must respect a continuous shift symmetry, broken to a discrete one only by its small mass and self-interactions. This leads to interactions in the form of higher-dimensional operators suppressed by the scale f_a, i.e., $\mathcal{L} \supset J^\mu \, \partial_\mu a/f_a$, where J^μ is a Standard Model current. Hence, the axion's small mass and coupling-strength are both related to the size of f_a, which is constrained to be much larger than the electroweak scale. At energies well below the electroweak scale, these interactions include

$$\mathcal{L} \supset c_\gamma \, \frac{a}{f_a} \, F_{\mu\nu} \, \widetilde{F}^{\mu\nu} + c_g \, \frac{a}{f_a} \, G^a_{\mu\nu} \, \widetilde{G}^{a\,\mu\nu} + c_\psi \, \frac{\partial_\mu a}{f_a} \, \bar{\psi} \, \gamma^\mu \gamma^5 \, \psi \; , \qquad\qquad 1.$$

where $F_{\mu\nu}$ and $G^a_{\mu\nu}$ are the photon and gluon field-strengths, respectively; $\widetilde{F}^{\mu\nu}$ and $\widetilde{G}^{a\,\mu\nu}$ are the dual field-strength tensors; ψ is the Dirac field for a Standard Model fermion; and c_γ, c_g, and c_ψ are model-dependent dimensionless coefficients.

For the spin-1 case, the theory of a vector field coupling to Standard Model currents J^μ is ill-behaved at high energies unless J^μ is conserved at the quantum level; otherwise, the coupling of the longitudinal mode is enhanced at high energies, which is strongly constrained by existing searches (25, 26). The only fully-conserved (i.e. anomaly-free) currents are those corresponding to electromagnetism and baryon-minus-lepton-number. In this work, we focus on the former case, which most naturally arises in models of kinetically-mixed dark photons.[1] Here, the A'_μ interacts with the Standard Model photon A_μ through a renormalizable operator that couples the two field-strengths (29). In a particular basis choice, this leads to an interaction with the electromagnetic current $J^\mu_{\rm em}$ of the form

$$\mathcal{L} \supset -(A_\mu + \epsilon \, A'_\mu) \, J^\mu_{\rm em} \; , \qquad\qquad 2.$$

---

[1] For a detailed review of dark photon phenomenology across a wide range of masses, see Refs. (27, 28).

where $\epsilon \ll 1$ is the dimensionless kinetic-mixing parameter. Note that $\epsilon \ll 1$ is technically natural since $\epsilon \neq 0$ breaks the combination of dark and visible charge conjugation symmetries to its diagonal subgroup. As we will describe further below, laboratory searches for dark photons are typically easier in their implementation, making the experimental situation quite complementary to those searching for electromagnetically-coupled axions.

2.2. Targets

Here, we expand upon the notion of "theory targets," i.e., regions of parameter space that are theoretically motivated. We begin with the so-called QCD axion. In this case, the axion arises as the Goldstone mode of a new spontaneously-broken Peccei-Quinn global $U(1)_{PQ}$ symmetry (30, 24, 31, 32). New fields coupled to QCD give rise to a mixed-anomaly under $U(1)_{PQ}$ and the $SU(3)_C$ gauge group. In turn, this results in a coupling of the QCD axion to gluons, which compared to Eq. 1 we rewrite as

$$\mathcal{L} \supset \frac{a}{f_a} \frac{\alpha_s}{8\pi} G^a_{\mu\nu} \widetilde{G}^{a\,\mu\nu} \, , \qquad\qquad 3.$$

where f_a is the reduced axion decay constant and α_s is the strong fine-structure constant. Below the QCD scale, this interaction generates a potential and mass for the axion (33),

$$m_a \simeq 5.7 \ \mu\text{eV} \times \left(10^{12} \ \text{GeV}/f_a\right) \, . \qquad\qquad 4.$$

Over cosmological timescales, the axion field relaxes to its minimum at which parity and time-reversal symmetry is preserved. The QCD axion thus provides a dynamical explanation for why the parity and time-reversal violating electric dipole moment (EDM) of the neutron is small, at least 10 orders of magnitude below naive expectations (34, 35).

Although Eqs. 3 and 4 imply a direct relationship between the mass m_a and the couplings proportional to $1/f_a$ for the QCD axion, there are models which modify this relationship. For instance, introducing $\mathcal{N} \gg 1$ copies of the Standard Model (and axion) that obey a $\mathbb{Z}_\mathcal{N}$ exchange symmetry gives a QCD-axion with values of $m_a f_a$ that are exponentially smaller by $2^{-\mathcal{N}}$, compared to Eq. 4 (36, 37, 38). However, this comes at the cost of a $1/\mathcal{N}$ linear tuning, which selects our sector as the one where parity and time-reversal symmetry violation is dynamically relaxed to zero.

Compared to the gluon coupling in Eq. 3, the QCD axion's coupling to photons is more model-dependent. This interaction has contributions both from Eq. 3, which induces a mixing between the axion and the neutral pion, as well as any additional field content charged under $U(1)_{PQ}$ and electromagnetism. Parameterizing the interaction as

$$\mathcal{L} \supset -\frac{g_{a\gamma\gamma}}{4} a F_{\mu\nu} \widetilde{F}^{\mu\nu} \, , \qquad\qquad 5.$$

the coupling coefficient $g_{a\gamma\gamma}$ is related to the additional particle content of the model by

$$g_{a\gamma\gamma} \simeq \frac{\alpha_{\text{em}}}{2\pi f_a} \left(\frac{E}{N} - 1.92\right) \simeq 2 \times 10^{-16} \ \text{GeV}^{-1} \times \left(\frac{m_a}{1 \ \mu\text{eV}}\right) \left(\frac{E}{N} - 1.92\right) \, , \qquad 6.$$

where E and N are the integer coefficients of the $U(1)_{PQ} \times U(1)_{EM}^2$ and $U(1)_{PQ} \times SU(3)_C^2$ anomalies, respectively, the term involving "1.92" is a recent estimate of the contribution from pion mixing (33), and in the second equality we used the relation of Eq. 4.

Two benchmark models for the QCD axion are the KSVZ axion (39, 40) and DFSZ axion (41, 42), corresponding to $E/N = 0$ and $E/N = 8/3$, respectively, yielding

$$|g_{a\gamma\gamma}| \simeq \left(\frac{m_a}{1\ \mu\text{eV}}\right) \times \begin{cases} 3.9 \times 10^{-16}\ \text{GeV}^{-1} & (\text{KSVZ} ,\ E/N = 0) \\ 1.5 \times 10^{-16}\ \text{GeV}^{-1} & (\text{DFSZ} ,\ E/N = 8/3) . \end{cases} \qquad 7.$$

Most experiments choose to focus on these two models when defining the range of interesting parameter space for the QCD axion. There are various reasons for this. The first one is largely historical. The KSVZ and DFSZ theories were introduced many decades ago, only a few years after Peccei and Quinn's first paper on the subject (24), and so are now considered the classic examples of the QCD axion. Another reason is a slight theoretical bias. DFSZ models are representative of many Grand Unified Theories, although there exist many counterexamples. The final reason is due to practical limitations. As we will discuss below, experiments often need to operate many runs in order to scan over a wide range of possible masses. Due to the time-consuming nature of these endeavors and the demands of funding agencies to outline an attainable and well-defined experimental program, collaborations have used the DFSZ prediction as a natural stopping point when defining their scope. However, it is a simple exercise to construct a model with much smaller $g_{a\gamma\gamma}$. For instance, taking $E/N = 2$ gives

$$g_{a\gamma\gamma} \simeq 1.6 \times 10^{-17}\ \text{GeV}^{-1} \times (m_a/\mu\text{eV}) \quad (E/N = 2) , \qquad 8.$$

an order of magnitude below the DFSZ prediction.

By contrast, the target theory space for dark photons is less sharply defined. This is due to the fact that unlike the dimension-five axion couplings, dark photons interact through a marginal dimension-four operator, and are therefore only logarithmically sensitive to the scale of new physics that generates this coupling. More concretely, assuming that ϵ vanishes at high energies, loops of particles charged under both the dark photon and electromagnetism radiatively generate a kinetic mixing of size

$$\epsilon \simeq \frac{e\,e'}{16\pi^2} \sum_i Q_i\,Q_i' \log\frac{\mu^2}{M_i^2} , \qquad 9.$$

where e and e' are the electromagnetic and A' gauge coupling, the sum runs over all particles of mass M_i charged under both sectors with visible and dark charge Q_i and Q_i', respectively, and μ is the renormalization scale (29, 43). Barring cancellations, and assuming that $e' \sim e$, this motivates kinetic mixing values of $\epsilon \sim 10^{-3}$, independent of the scale of new physics. However, it is simple to construct theories where $\epsilon \ll 10^{-3}$ (44). This is the case, for instance, if $e' \ll e$, or instead if this interaction arises from mixing between a non-abelian and abelian group, such that it is generated by a higher-dimensional operator suppressed by the mass-scale of new particles charged under both sectors (45).

Cosmological considerations can also be used to motivate particular regions of parameter space. However, since early universe production mechanisms are not the focus of this review, we simply refer the reader to the recent work of, e.g., Refs. (46, 47). While cosmology can motivate particular regions of parameter space (assuming that such particles make up the entirety of the dark matter), it is also possible that the dark matter density in the Solar System deviates drastically from its average galactic value $\rho_{\text{DM}} \simeq 0.4\ \text{GeV/cm}^3$ (48). For instance, axion self-interactions can lead to substructure in the form of large overdensities ("miniclusters") surrounded by significant underdensities ("minivoids") (49, 50, 51, 52).

The rate at which Earth would encounter such a minicluster is likely quite low but depends on the details of the theory and formation mechanism, and is subject to large theoretical uncertainties regarding the survival rate of such objects in the Milky Way. Regardless, the possibility that an $\mathcal{O}(1)$ fraction of the dark matter is bound up in rare dense objects could mean that the effective value of ρ_{DM} for terrestrial experiments would be much smaller than the conventional value of $\rho_{\mathrm{DM}} = 0.45$ GeV/cm^3 adopted within the community of axion experimentalists. It is also plausible that axions or dark photons make up a small sub-component of the dark matter. Either of these cases highlight the importance of exploring signals weaker than that predicted by the canonical homogeneous dark matter scenario.

3. Dark Matter in the Lab

In this section, we outline various laboratory search strategies for axions and dark photons, assuming that they make up the dark matter of our galaxy. Before delving into the details of the various types of signals, we begin with a brief overview of the theoretical description of ultralight bosonic dark matter in the laboratory. Although the mass of a dark matter particle is largely unconstrained, its mass density can be inferred from astrophysical observations, with an average value in the solar neighborhood $\rho_{\mathrm{DM}} \simeq 0.4$ GeV/cm^3 (48). As a result, sub-eV dark matter has a much larger number density $n_{\mathrm{DM}} \simeq \rho_{\mathrm{DM}}/m_{\mathrm{DM}}$ than traditional weak-scale dark matter, which leads to qualitatively different phenomenology in the laboratory. In particular, considering the typical galactic dark matter velocity $v_{\mathrm{DM}} \sim 10^{-3}$ and the associated de Broglie wavelength $\lambda_{\mathrm{DM}} \sim 2\pi/(m_{\mathrm{DM}} v_{\mathrm{DM}})$, the dark matter occupancy per de Broglie volume $N_{\mathrm{occ}} = n_{\mathrm{DM}} \lambda_{\mathrm{DM}}^3$ is much larger than unity for $m_{\mathrm{DM}} \ll 30$ eV.

Sub-eV dark matter thus has macroscopic phase space occupancy, leading to an interesting interplay of classical and quantum effects. Feebly-coupled ultralight axion or dark photon dark matter fields may be described as a nonrelativistic classical field oscillating at the dark matter mass,

$$a \simeq \frac{\sqrt{2\rho_{\mathrm{DM}}}}{m_a} \cos\left(m_a(t - \mathbf{v}_{\mathrm{DM}} \cdot \mathbf{x})\right) \quad , \quad |\boldsymbol{A}'| \simeq \frac{\sqrt{2\rho_{\mathrm{DM}}}}{m_{A'}} \cos\left(m_{A'}(t - \mathbf{v}_{\mathrm{DM}} \cdot \mathbf{x})\right) , \qquad 10.$$

coherent over a length scale and timescale of

$$\lambda_{\mathrm{DM}} \simeq 700 \text{ m} \times \left(\frac{1 \ \mu\mathrm{eV}}{m_{\mathrm{DM}}}\right) \quad , \quad \tau_{\mathrm{DM}} \simeq 3 \text{ ms} \times \left(\frac{1 \ \mu\mathrm{eV}}{m_{\mathrm{DM}}}\right) , \qquad 11.$$

respectively. Similar results are obtained with a full quantum treatment of the axion field using the formalism of density matrices and open quantum systems (53, 54, 55, 56); one advantage of this formalism is the ability to precisely specify quantities such as the coherence length λ_{DM} and time τ_{DM}, which can be defined through the field autocorrelation function.

Experiments aiming to detect axion or dark photon dark matter in the lab will almost invariably measure power spectra of, e.g., laboratory fields, which will end up being proportional to the dark matter two-point function. It is worth noting that it is common in the literature to rewrite the coherence time as $\tau_{\mathrm{DM}} \sim Q_{\mathrm{DM}}/m_{\mathrm{DM}}$ where

$$Q_{\mathrm{DM}} \sim v_{\mathrm{DM}}^{-2} \sim 10^6 \qquad 12.$$

is an effective quality factor of the dark matter field. In this sense, Q_{DM} does not have anything to do with dissipation; instead, it describes the dark matter field's spectral width

$\sim m_{\rm DM}/Q_{\rm DM}$ in frequency-space. Sub-eV dark matter also offers the appealing prospect of being able to immediately measure the full 3-dimensional velocity distribution of dark matter in our galaxy following a detection (57, 58, 59), as well as daily modulation from the dark photon polarization (28). This is to be contrasted with WIMP experiments, which are rare event searches and thus take much more time to map out the velocity distribution.

3.1. Electromagnetic Searches

In this section, we review experimental techniques to probe electromagnetically-coupled axion and dark photon dark matter, defined in Eqs. 5 and 2, respectively. As we will see below, both can lead to effective source terms in Maxwell's equations. Thus, searches for either model are highly synergistic, with the main difference often being that axion experiments typically require applied magnetic fields, whereas dark photon searches do not.

Let us begin with a description of axion electrodynamics. Experimentally, the most readily accessible axion coupling in laboratory experiments is its interaction with photons. Indeed, the earliest experimental searches for axions with sensitivity to f_a well above the electroweak scale were electromagnetic cavity experiments dating back to the late 1980s (60, 61, 62). In the last decade, there has been a flourishing of new experimental ideas, many of which have already come to fruition and begun taking data.

The effect of the axion-photon coupling $g_{a\gamma\gamma}$ is most easily seen by considering how it changes Maxwell's equations. In Gauss's and Ampère's laws, the axion field enters as an effective charge and current density in the presence of electromagnetic fields,

$$\rho_{a\gamma} \equiv -g_{a\gamma\gamma}\, \boldsymbol{B} \cdot \nabla a \quad , \quad \boldsymbol{J}_{a\gamma} \equiv -g_{a\gamma\gamma}\left(\boldsymbol{E} \times \nabla a - \boldsymbol{B}\, \partial_t a\right) . \qquad 13.$$

In an experiment searching for axion dark matter, the second term in $\boldsymbol{J}_{a\gamma}$ dominates, since from Eq. 10 the spatial gradient of the axion field is suppressed by the small dark matter velocity $v_{\rm DM} \sim 10^{-3}$. Thus, in the presence of a large background laboratory magnetic field $\boldsymbol{B}_0$, axion dark matter sources an effective current density $\boldsymbol{J}_{a\gamma} \simeq g_{a\gamma\gamma}\, \boldsymbol{B}_0\, \partial_t a$, which in turn generates small response fields proportional to $g_{a\gamma\gamma}$ across a narrow frequency band of width $m_a/Q_{\rm DM}$ near m_a. Such signal fields can be significantly enhanced in amplitude through the use of electromagnetic resonant detectors, such as cavities and LC circuits.

Kinetically-mixed dark photons also modify Maxwell's equations. To describe physical effects, it is often more convenient to change basis from that of Eq. 2 to the so-called "visible" and "invisible" field basis, which can be identified by noting that the visible linear combination of fields $A_{\rm vis} \simeq A + \epsilon A'$ couples to Standard Model currents, whereas the invisible linear combination $A_{\rm inv} \simeq A' - \epsilon A$ is completely decoupled ($A_{\rm vis}$ is the field that is, e.g., screened by electromagnetic shields). The dark photon field sources an effective charge and current density for visible fields (63, 64)

$$\rho_{A'} \equiv -\frac{\epsilon\, m_{A'}^2}{1 - \epsilon^2}\, \phi' \quad , \quad \boldsymbol{J}_{A'} \equiv -\frac{\epsilon\, m_{A'}^2}{1 - \epsilon^2}\, \boldsymbol{A}' , \qquad 14.$$

where we decomposed the dark photon field as $A'^{\mu} = (\phi', \boldsymbol{A}')$. For a massive vector field, charge continuity demands that $\partial_\mu A'^{\mu} = 0$,[2] such that the dark scalar potential is parametrically smaller than the dark vector potential, $\phi' \sim v_{\rm DM}\, |\boldsymbol{A}'| \ll |\boldsymbol{A}'|$. From the expressions

---

[2] Note that for a massive vector field, this is actually not a gauge choice, but is instead a consequence of conservation of dark charge J'^{μ} and arises from the equations of motion for A'.
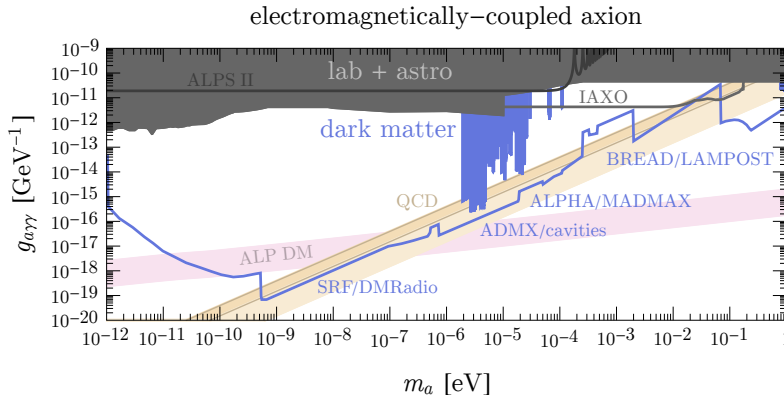
Figure 1

A summary of the parameter space for electromagnetically-coupled axions (Eq. 5), in the plane spanned by the axion-photon coupling $g_{a\gamma\gamma}$ and axion mass m_a. Gray regions or lines do not assume that axions make up the dark matter, whereas blue ones assume axions comprise the full galactic dark matter density. Shaded regions correspond to existing limits, whereas lines correspond to the projected sensitivity of proposed experiments. Labels refer to experiments discussed throughout this review. The darker orange band denotes the range of couplings and masses as motivated by the canonical QCD axion models of Eq. 7, whereas the bottom of the light orange region corresponds to the QCD axion model of Eq. 8. Along the pink band, axion-like particle production through the misalignment mechanism with an $\mathcal{O}(1)$ initial misalignment angle is consistent with the observed dark matter energy density (46, 47).

above, we see that the A' decouples from the Standard Model in the massless limit $m_{A'} \to 0$, which is due to the fact that our visible photon is simply the linear combination $A + \epsilon A'$ in Eq. 2 (an exception to this is if there are dark sector particles directly charged under the A', as in models of millicharged particles, which couple to both sectors (65, 66)). Hence, any calculation that implies sensitivity to a massless dark photon (in the absence of dark charges) should be met with skepticism.

From Eq. 14 we see that the dominant effect for dark photon dark matter is also an effective current density $\boldsymbol{J}_{A'} \simeq -\epsilon m_{A'}^2 \, \boldsymbol{A}'$, now aligned along the polarization of the dark photon field rather than an external magnetic field. Indeed, unlike in the case of the axion, the dark photon signal will appear whether or not the magnetic field is on. As a result, the sensitivity of experiments searching for electromagnetically-coupled axion dark matter can often be recast in terms of dark photon dark matter (28) (so long as care is taken in regards to any magnetic field veto). Comparing the form of the effective currents in Eqs. 13 and 14 implies that an axion experiment employing a magnetic field of strength B_0 that is sensitive to a coupling $g_{a\gamma\gamma}$ is typically sensitive to dark photons of the same mass with a kinetic mixing of $\epsilon \sim g_{a\gamma\gamma} B_0 / m_{\rm DM}$.[3] Especially in cases where the experimental apparatus involves superconducting elements, a dedicated dark photon search without the external B-field often involves fewer technical complications.

The important scale in electromagnetic axion and dark photon dark matter experiments

---

[3]A notable exception is a toroidal axion experiment, the geometry of which is maximally mismatched to a dark photon search (28).

is the dimensionless quantity $m_{\mathrm{DM}}\, L_{\mathrm{exp}}$, involving the dark matter mass and the size of the experiment L_{exp}, which determines the relative importance of retarded-time and radiation effects.[4] Although not every experimental strategy is perfectly captured by the following categorization, three regimes motivate qualitatively different experimental techniques: 1) In the quasi-static regime ($m_{\mathrm{DM}}\, L_{\mathrm{exp}} \ll 1$), retarded-time effects are negligible, such that the dark matter effective current sources a quasi-static signal magnetic field. 2) In the cavity regime ($m_{\mathrm{DM}}\, L_{\mathrm{exp}} \sim 1$), retarded-time effects are maximal, i.e., $\partial_t \boldsymbol{E}$ and $\nabla \times \boldsymbol{B}$ are comparable in magnitude in Ampère's Law. 3) In the radiation regime ($m_{\mathrm{DM}}\, L_{\mathrm{exp}} \gg 1$), the displacement current term $\partial_t \boldsymbol{E}$ dominates over $\nabla \times \boldsymbol{B}$.

At a practical level, the boundary between these regimes is set by the size of typical state-of-the-art conducting cavities ($L_{\mathrm{exp}} \sim \mathrm{cm} - \mathrm{m}$, corresponding to $L_{\mathrm{exp}}^{-1} \sim$ GHz frequencies), as well as by the demands of the readout, with GHz corresponding to the transition between DC SQUID readout at lower frequencies and microwave electronics at higher frequencies. As such, we will organize our discussion of dark matter experiments searching for electromagnetic couplings with respect to the GHz scale. A high-level overview of existing limits and projected sensitivities of future experiments is shown in Figs. 1 and 2.

Finally, let us provide a general parametric estimate for the signal power which can be applied to many of the setups described below. The dark matter effective current $\boldsymbol{J}_{\mathrm{DM}} = \boldsymbol{J}_{a\gamma}$ or $\boldsymbol{J}_{A'}$ will deposit power into an experiment operating at a frequency ω_{exp} (in general, $\omega_{\mathrm{exp}} \neq m_a$). In any of the three frequency regimes, the signal power in many experimental setups can be written schematically as

$$
P_{\mathrm{sig}} \sim \left(\eta\, J_{\mathrm{DM}}\right)^2 L_{\mathrm{exp}}^4 \, \min\left(1\,,\, \omega_{\mathrm{exp}}\, L_{\mathrm{exp}}\right) \, \min\left(Q_{\mathrm{exp}}\,,\, \frac{\omega_{\mathrm{exp}}}{m_{\mathrm{DM}}}\, Q_{\mathrm{DM}}\right) . \qquad 15.
$$

Here, $\eta \lesssim 1$ is a dimensionless form factor quantifying the overlap between the dark matter field and the experimental setup, such that $\eta \sim \mathcal{O}(1)$ in optimized geometries; note that η can be much smaller for, e.g., large open dish antennas with $\eta \sim \left(\omega_{\mathrm{exp}}\, L_{\mathrm{exp}}\right)^{-1} \ll 1$. Q_{exp} is the quality factor of the detector, which is $\mathcal{O}(1)$ for open setups, but can be $\gg 1$ for cavity or lumped-element resonators. Furthermore, we have ignored details pertaining to the aspect ratio of the system; for instance, for experiments consisting of spaced layers of dielectrics, L_{exp}^4 should be replaced by area $\times$ length^2 in Eq. 15. Although the integrated signal power in Eq. 15 is independent of the detector's quality factor for $Q_{\mathrm{exp}} \gtrsim \left(\omega_{\mathrm{exp}}/m_{\mathrm{DM}}\right) Q_{\mathrm{DM}}$, the sensitivity of a resonant setup is often still enhanced for even larger Q_{exp}. This is due to the fact that the total noise power integrated over the resonator bandwidth $\sim \omega_{\mathrm{exp}}/Q_{\mathrm{exp}}$ is suppressed compared to P_{sig} if, e.g., the noise temperature is independent of Q_{exp}. In this case, the signal-to-noise ratio generally scales as the geometric mean $\sqrt{Q_{\mathrm{exp}}\, Q_{\mathrm{DM}}}$ for a fixed scanning time to cover an e-fold in dark matter mass.

3.1.1. GHz frequencies.
The first experiments that had plausible direct detection sensitivity to dark matter axions were GHz microwave cavity experiments dubbed "haloscopes" (60, 61, 62), which have evolved into the modern ADMX program and influenced the design of other newer experiments. These experiments employ magnetic fields applied to cavities tuned to the dark matter frequency, such that $\omega_{\mathrm{exp}} \sim L_{\mathrm{exp}}^{-1} \sim m_{\mathrm{DM}}$. Independent of the magnetic

---

[4]To be more precise, retarded-time effects are typically governed by the physical distance a current must travel around a device, so for a cylindrical geometry, L_{exp} is the circumference rather than the radius (see Ref. (67) for an example).
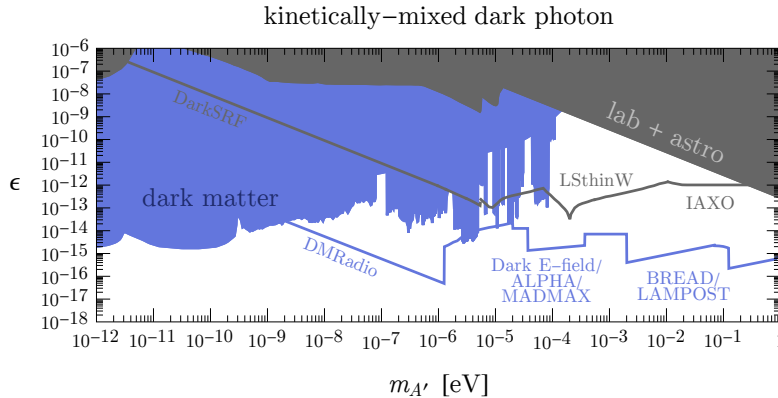
Figure 2

As in Fig. 1, but for the kinetically-mixed dark photon parameter space (Eq. 2), spanned by the kinetic mixing parameter ϵ and the dark photon mass $m_{A'}$.

field, these setups have sensitivity to dark photon dark matter as well. The narrow-band nature of such experiments requires constant operations to tune to new frequencies, and often the experimental focus is on maintaining live-time while collecting data from a system that has many moving components. The key figure of merit for cavity experiments is the dark matter frequency scan rate,

$$\frac{d\omega_{\text{exp}}}{dt} \propto Q_L \, Q_{\text{DM}} (\rho_{\text{DM}} \, V_{\text{exp}} \, \eta/T_n)^2 \times \begin{cases} (g_{a\gamma\gamma} \, B_0)^4 & \text{(axion)} \\ \epsilon^4 & \text{(dark photon)} \, , \end{cases} \qquad 16.$$

where Q_L is the loaded cavity quality factor, V_{exp} is the cavity volume, η is a mode-overlap form factor, and T_n is the effective noise temperature. It is important to note that Eq. 16 holds even when $Q_L \gg Q_{\text{DM}}$; consistent with Eq. 15, there is no penalty for having an intrinsic cavity linewidth narrower than the dark matter, so long as tuning steps are taken with fractional width Q_{DM}^{-1} rather than Q_L^{-1} (68, 69, 70).

Over the last decade there has been a steady progression of experiments that have come online, and new ones are progressing further with R&D demonstrator and conceptual designs. Two experiments, ADMX and CAPP, have matured to the point of searching down to the QCD line over a fairly wide frequency range. As of this writing, ADMX-G2 has covered $(0.65 - 1.02)$ GHz (71, 72, 73) and CAPP has covered $(1.025 - 1.185)$ GHz (74) at or near DFSZ sensitivity. Both experiments plan to continue scanning with existing technology: copper cavities with one or more tuning rods, large-bore magnets with modest fields (NbTi at 7.8 T for ADMX, and 10.8 T for CAPP-MAX), and cryogenic amplification with current-pumped or flux-pumped Josephson Parametric Amplifiers (JPAs) running as a linear amplifier near the quantum limit.

One of the primary research directions that has borne fruit is the development of field-tolerant SRF cavities. Though superconducting accelerator cavities have quality factors as large as $Q \gtrsim 10^{11}$ (75), it is generally believed that RF losses due to flux vortex motion degrade surface loses at high-field to below that of copper. Fortunately, these concerns are not relevant for dark photon searches which do not require an external B-field, and Ref. (70) recently set the strongest constraints on ϵ at any dark photon mass using a

cavity with $Q_L = 4.7 \times 10^9$, obtaining $\epsilon < 1.5 \times 10^{-16}$ in a narrow band around $m_{A'} = 5.35 \ \mu$eV. That said, SRF cavities made from Nb$_3$Sn films demonstrated $Q \sim 5 \times 10^5$ in a 6 T magnetic field (76), and work is continuing to use Nb$_3$Sn coatings to increase Q for superconducting cavities in high fields. Other ideas include a variety of material coatings on various substrates (for example, NbTi on Cu, Nb3Sn on Nb, Nb3Sn on Cu, or ReBCO high-temperature superconductor tape), which have been demonstrated in empty cavities (77, 78, 79). Tunable systems using these coatings are beginning to be deployed (80, 81) with quality factors approaching $\sim 10^6$ being demonstrated.

3.1.2. Low Frequencies (below GHz).
Since the lowest resonant frequency of a cavity scales as its inverse size, probing sub-μeV masses with the cavity haloscopes discussed above requires prohibitively large systems. Various experimental schemes have been proposed to overcome this.

One strategy involves the use of lumped-element LC circuits as electromagnetic resonators; their resonant frequency is not directly tied to their inverse geometric size, allowing them to operate in the quasi-static limit, $\omega_{\rm exp} = 1/\sqrt{LC} \ll 1/L_{\rm exp}$. As for cavity haloscopes, such a setup requires tuning the resonant frequency to the dark matter mass $\omega_{\rm exp} \simeq m_{\rm DM}$, as well as employing an external magnetic field to search for axion dark matter. A large pickup inductor can be used to resonantly amplify the magnetic field sourced by either the axion or dark photon effective current. This approach is being undertaken by the DMRadio collaboration (82), which plans on developing large LC resonators with quality factors of $Q_{\rm LC} \sim Q_{\rm DM} \sim 10^6$ with the ultimate goal of probing QCD axion dark matter in the MHz − GHz frequency range. Implementing this strategy requires a large high-Q sapphire capacitor which is tunable over decades of capacitance to parts-per-million precision, which DMRadio is currently developing. The ADMX SLIC experiment has demonstrated the viability of this strategy over a narrow frequency range, using piezoelectric tuning of an LC circuit inside a solenoidal magnet (83). At the highest frequencies, approaching the cavity regime with $m_{\rm DM} L_{\rm exp} \sim 1$, the lumped-element approximation breaks down and inductors develop a capacitive impedance (67), which induces parasitic resonances and requires several inductive pickup sheaths of various sizes to fully cover the desired mass range (84). In the absence of a tunable capacitor, one can still use purely inductive readouts to perform a broadband search, as was pioneered by ABRACADABRA (85) and SHAFT (86) (a non-tunable capacitor would improve sensitivity even off-resonance (68)).

Heterodyne searches based on frequency up-conversion schemes have also been proposed in Refs. (69, 87, 88) to probe sub-GHz QCD axion dark matter. These setups employ a SRF cavity with two nearly-degenerate tunable modes, referred to as the "pump mode" and "signal mode." The cavity pump mode is driven at angular frequency $\omega_0 \sim$ GHz. Since the axion effective current $\boldsymbol{J}_{a\gamma}$ involves the product of the pump magnetic field and the axion field, $\boldsymbol{J}_{a\gamma}$ oscillates at the beat frequencies $\omega_{\rm exp} = \omega_0 \pm m_a$. Thus, if the signal mode is tuned to the nearby frequency $\omega_1 \simeq \omega_0 \pm \Delta\omega$ offset by $\Delta\omega \ll \omega_0$, then axion dark matter oscillating at the frequency splitting $m_a \simeq \Delta\omega$ can resonantly drive power from the pump to the signal mode. This approach is currently being pursued at Fermilab (89). Compared to static-field lumped-element resonators, the main qualitative difference here arises from the fact that the applied magnetic field is in the form of a time-dependent driven mode of the cavity, which upconverts the low-frequency axion into a higher frequency RF signal, $\omega_{\rm exp} \gg m_a$. As can be inferred from Eq. 15, this has two important implications. First, in general the integrated signal power $P_{\rm sig}$ saturates once the coherence time of

the resonator overcomes that of the axion field. In an up-conversion setup, this occurs once $Q_{\rm exp} \gtrsim ({\rm GHz}/m_a)\,Q_a \gg 10^6$, such that $P_{\rm sig}$ is enhanced by the large quality factors achievable with SRF cavities (as large as $Q_{\rm exp} \sim {\rm few} \times 10^{11}$) (75). Second, Lenz's law implies that $P_{\rm sig}$ is dictated by $\partial_t J_{a\gamma}$. Thus, the signal power in a static-field setup is suppressed by the small axion mass $P_{\rm sig} \propto m_a$ for $m_a \ll L_{\rm exp}^{-1} \sim \mu{\rm eV}$. However, by oscillating the applied field in an up-conversion experiment, this suppression is undone.

Either of these low-frequency search strategies needs to contend with an irreducible background arising from the large number of thermal photons at finite temperature. In this case, thermal fluctuations preclude the usefulness of techniques such as photon counting and squeezing. However, for a scanning experiment, lowering the readout noise well below the standard quantum limit (which dominates off-resonance) enhances the signal-to-noise ratio by broadening the so-called "sensitivity bandwidth" to be much greater than the resonator bandwidth (68, 69, 90). Thus, as opposed to photon counting, quantum metrology related to low-noise phase-sensitive readout of voltage (91), which allows the frequency to be determined, could potentially further enhance the scan rate of these setups.

An effect closely related to the heterodyne one arises from modifications to the photon's dispersion relation. In an axion dark matter background, the phase velocity of left- and right-polarized light with frequency ω_0 is shifted by $\delta v \simeq \pm g_{a\gamma\gamma}\,\sqrt{2\rho_{\rm DM}}/(2\omega_0)$, which is equivalent to a rotation of linear polarized light. Experimental setups based on optical interferometry have been proposed in, e.g., Refs. (92, 93), which rely on the phase difference accumulated by the different circular polarizations. Such schemes could cover new parameter space 1–2 orders of magnitude beyond existing astrophysical bounds.

3.1.3. High frequencies (GHz and above).

At high frequencies, at least two challenges for the resonant cavity approach become apparent. First, from the scan rate in Eq. 16, the form factor η is $\mathcal{O}(1)$ only when the dark matter Compton wavelength is of order the cavity size, which requires a cavity volume of $V_{\rm exp} \sim 1/m_{\rm DM}^3$, limiting the sensitivity for larger masses. Second, the parametric amplifiers used for cavity searches no longer operate at THz frequencies and above, so a qualitatively different readout is required. Here, we discuss approaches to mitigate these challenges.

At frequencies not too far above 1 GHz, the loss in sensitivity from the reduced volume of a single smaller cavity can be counteracted with lower readout noise. Strategies based on quantum metrology are actively being developed in this frequency range, which may also prove more generally useful in other regimes. For instance, HAYSTAC (94, 95) has pioneered the use of low-noise squeezed-state JPAs to increase the effective cavity bandwidth, thus enhancing the scan rate at each frequency step beyond that implied by the standard quantum limit. Currently, HAYSTAC is the only axion experiment to have demonstrated operation beyond the standard quantum limit, and the factor of $\sim 2-3$ in scan rate gained by squeezing is currently limited by the state of quantum technology, offering a promising opportunity for improvement in the future. HAYSTAC has already taken and analyzed data in the $(4-5)$ GHz frequency range, and expects to cover $(10-12)$ GHz in future runs. Other approaches involve single-photon detection (96) as a readout strategy, where the occupation number of photons in a cavity may be non-destructively measured through its effect on the frequency of a qubit oscillation. Indeed, Ref. (96) has already demonstrated single-photon detection as a viable strategy for dark photon detection, constraining $\epsilon < 1.7 \times 10^{-15}$ for dark photon dark matter in a narrow band around $m_{A'} \simeq 24.86\ \mu{\rm eV}$. An alternate strategy involves quantum-mechanically enhancing the signal by preparing a superconducting qubit

in a non-classical Fock state (97). The challenge of extending these latter strategies to axion detection involves maintaining qubit operation near a large magnetic field (98).

Another approach involves maintaining a large effective volume at higher frequencies. For instance, ADMX-EFR (99) proposes to read out 18 small cavities simultaneously in a 9.4 T magnet to cover the $(2-4)$ GHz frequency range. One may also consider creating a "metamaterial" consisting of a dense array of conducting wires in order to modify the photon plasma frequency ω_p, thus facilitating resonant conversion when $\omega_p \sim m_{\rm DM}$ and decoupling the experimental volume from the form factor (100). The ALPHA experiment will use this "plasma haloscope" setup to search in the $(5-50)$ GHz range; performance of the metamaterial has been validated recently at ~ 10 GHz (101).

Moving to higher frequencies, MADMAX (102) and DALI (103) use an array of dielectric disks to exploit electromagnetic boundary conditions. In the presence of the dark matter effective current, electric fields must be induced at the disk boundary, producing radiation at a frequency $\omega_{\rm exp} \simeq m_{\rm DM}$. Many such disks may be placed inside a coherence length, allowing the radiation to constructively interfere and generating either a broadband or narrow-band response function depending on the disc spacing. For instance, operating in the so-called "transparent mode," N disks of refractive index n and thickness $\pi/(n\,m_{\rm DM})$ are separated by a vacuum gap of thickness $\pi/m_{\rm DM}$. In this case, the outgoing radiation adds coherently, and the sensitivity bandwidth of the setup is roughly $\sim m_{\rm DM}/N$. Demanding that the total length of the experiment fits inside a coherence length ($N \lesssim 1/v_{\rm DM} \sim 10^3$) then leads to the optimal signal power scaling in Eq. 15. A MADMAX prototype with three sapphire disks in a 1.6 T B-field has recently taken first data, demonstrating a power boost factor of ~ 2500 from constructive interference from the disks and constraining an axion coupling of $g_{a\gamma\gamma} < 2 \times 10^{-11}$ GeV^{-1} in a narrow range of masses around $m_a \simeq 80$ μeV (104). This prototype was operated in the 10 GHz range and was thus able to use a similar readout to HAYSTAC; however, the full experiment, which aims for $(10-100)$ GHz, will likely need new readout strategies beyond the quantum limit at the highest frequencies (102).

A similar strategy can be employed with much smaller dielectric spacing, read out with superconducting nanowire single-photon detectors (SNSPDs) to probe near-optical frequencies. This is the strategy pursued by, e.g., LAMPOST (105), which leverages SNSPDs with extremely low dark rates in a commensurately scaled-down geometry involving several μm-thick alternating layers fused into a "dielectric stack." First data has been taken without the magnetic field, constraining $\epsilon \lesssim 10^{-12}$ for dark photon masses of $m_{A'} \sim (0.7-0.8)$ eV (106); the dark rates for the SNSPDs were an impressive 6×10^{-6} Hz, corresponding to 4 total counts over the 180-hour exposure. Future runs aim to push toward masses of 10 meV, which is within the sensitivity band of lower-threshold SNSPDs but with potentially higher dark rates. A similar approach, MuDHI, uses a 23-layer dielectric stack with a single-photon avalanche detector at 1.5 eV and has set dark photon limits at $\epsilon \lesssim 10^{-10}$ (107).

Other approaches have eschewed resonant scanning in favor of fundamentally broadband setups with sensitive photon detectors. For instance, the BREAD collaboration has revived an older approach using a dish antenna in a specialized parabolic geometry that focuses the dark matter-induced radiation onto a small detector area (108). Multiple readout techniques, including kinetic inductance detectors at $(0.1-1)$ THz, quantum capacitance detectors at $(1-10)$ THz, and SNSPDs at $(10-100)$ THz, are envisioned to cover several decades of axion masses down to the KSVZ target and potentially beyond. Broadband approaches have also been developed at GHz $-$ THz frequencies, such as the Dark E-field pilot experiment (109), which used a dipole antenna in a shielded room to search for the
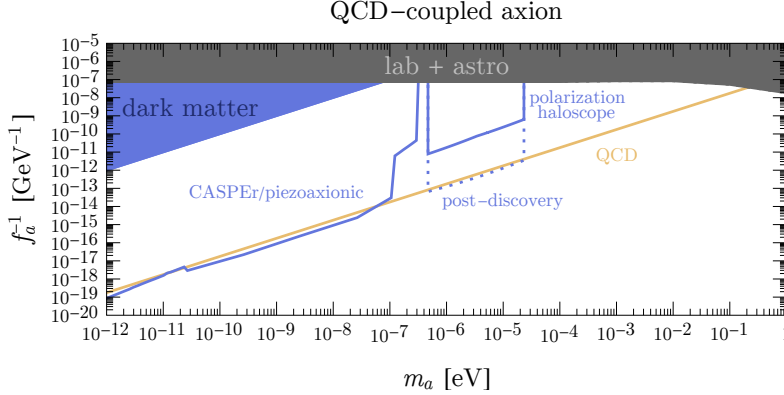
QCD−coupled axion

Figure 3

As in Fig. 1, but for the defining coupling of the QCD axion (Eq. 3), in the parameter space spanned by the inverse axion decay constant f_a^{-1} and the axion mass m_a. The orange line denotes the standard QCD axion relation of Eq. 4. The dotted blue line shows the reach for a polarization haloscope experiment which targets a single candidate QCD axion mass (112); this would be the case to definitively test whether a signal at an RF haloscope does indeed arise from the QCD axion.

electric field generated by dark photon dark matter.

Another broadband approach at higher frequencies leverages the development of low-noise targets for the detection of sub-GeV dark matter scattering. In particular, target materials hosting in-medium electronic (110) and phonon (111) excitations, are also sensitive to axion dark matter if these detectors are operated in strong magnetic fields, thus creating a "magnetized medium." In this case, the total signal rate is governed by the dielectric energy-loss function $P_{\text{sig}} \propto \text{Im}(-\varepsilon^{-1})$ involving the permittivity evaluated at frequency $\omega \simeq m_a$ (110), demonstrating that sensitivity to new parameter space is possible for $m_a \sim (0.1 - 10)$ eV, provided that existing dark counts are reduced compared to existing values.

3.2. QCD

Here, we give an overview of existing and proposed dark matter searches for the defining coupling of the QCD axion to gluons, Eq. 3. A summary of existing limits and projected sensitivities is shown in Fig. 3. For this coupling, the dark matter axion field is equivalent to an effective QCD theta angle oscillating at a frequency set by the dark matter mass,

$$\theta_a = \frac{a}{f_a} \simeq \frac{\sqrt{2\rho_{\text{DM}}}}{m_a f_a} \cos m_a t \simeq 4.3 \times 10^{-19} \cos m_a t \ , \qquad 17.$$

where we used Eq. 4 in the second equality. This gives rise to various effects that violate parity and time-reversal symmetry at low energies. One such effect is that the neutron acquires a non-vanishing *oscillating* electric dipole moment, $d_n \simeq (2.4 \times 10^{-3} \ e \ \text{fm}) \theta_a$, which generates a coupling between the neutron spin and an applied electric field $\boldsymbol{E}_0$.

The CASPEr-Electric experiment (113, 114) aims to search for this interaction with nuclear magnetic resonance (NMR) techniques. The induced electric dipole moment leads to a small oscillating nuclear polarization aligned with a background electric field $\boldsymbol{E}_0$, which can be read out with a precision electromagnetic sensor, such as a SQUID. For nuclear spins

initially polarized along an applied magnetic field $\boldsymbol{B}_0$ transverse to $\boldsymbol{E}_0$, the spin-response can be resonantly enhanced if the dark matter frequency matches the Larmor frequency, $m_a \simeq \gamma_n B_0$, where γ_n is the gyromagnetic ratio of the nucleon. As a result, this setup can scan over a range of axion masses by tuning B_0. The overall effect can be further amplified with the use of ferroelectric materials with large internal electric fields. The ultimate spin projection noise-limited reach of CASPEr-Electric can explore QCD axion dark matter in the $(10^{-12} - 10^{-7})$ eV mass range (see also Ref. (115)). A similar range of QCD axion masses could also potentially be covered by an experiment designed to search for the so-called "piezoaxionic" effect (116). In this case, the oscillating nuclear electric dipole moment couples to the mechanical stress of a nuclear spin-polarized piezoelectric crystal, which can be resonantly enhanced when the axion mass is close to a vibrational mode of the system.

Both of the aforementioned strategies are optimized for sub-GHz frequencies, corresponding to axion masses $m_a \lesssim 10^{-6}$ eV. In the case of CASPEr-Electric, this is due to the fact that resonance is achieved for $m_a \simeq \gamma_n B_0$, such that probing $m_a \gtrsim 10^{-6}$ eV would require magnetic fields greater than those accessible in the laboratory, $B_0 \gtrsim 10$ T. Furthermore, an experiment based on the piezoaxionic effect is optimal when m_a is comparable to a low-lying mechanical resonance, which for a large sample typically lies well below $\mathcal{O}(1)$ GHz in frequency, due to the small speed of sound. To probe $\gtrsim$ GHz frequencies, the so-called "polarization haloscope" has been proposed (112), which involves placing a nuclear spin-polarized dielectric in a conducting cavity. Analogous to the neutron electric dipole moment, Eq. 17 generates an oscillating atomic electric dipole moment d_A directed along the spin. The corresponding oscillating polarization density $P_{\mathrm{EDM}} \sim n_A d_A$ in a medium of atomic spin density n_A induces an electromagnetic current $\boldsymbol{J}_{\mathrm{EDM}} = \partial_t \boldsymbol{P}_{\mathrm{EDM}}$, which can resonantly excite the mode of a microwave cavity whose frequency is comparable to the axion mass. For the QCD axion, comparison between $\boldsymbol{J}_{\mathrm{EDM}}$ and $\boldsymbol{J}_{a\gamma}$ implies that the signal generated by the QCD coupling is typically a few orders of magnitude smaller (112). Regardless, a polarization haloscope could explore new parameter space at high frequencies, as well as definitively test whether a potential future signal seen at an experiment such as ADMX indeed arises from the QCD axion. In any of the experiments discussed in this section, achieving the sensitivity shown requires overcoming various experimental difficulties. This includes minimizing noise at low frequencies, as well as identifying optimal materials that can be prepared with large nuclear spin-polarization fractions and enhanced Schiff moments (thus allowing large internal electric fields).

Before concluding this section, we also note that the QCD axion can lead to effects that obey parity and time-reversal symmetry, but at higher-order in θ_a. For example, at $\mathcal{O}(\theta_a^2)$, there exist corrections to nucleon and pion masses (117), as well as the parity and time-reversal even interaction with photons, $\mathcal{L} \supset \mathcal{O}(10^{-4}) \, \theta_a^2 \, F_{\mu\nu} F^{\mu\nu}$ (118, 119). This interaction modifies the effective fine-structure constant, thus shifting atomic energy levels and potentially generating signals that can be searched for with atomic clock experiments. Since this interaction is parametrically suppressed compared to those linear in θ_a, such searches cannot probe parameter space corresponding to the canonical QCD axion. Regardless, these interactions represent qualitatively different types of signatures.
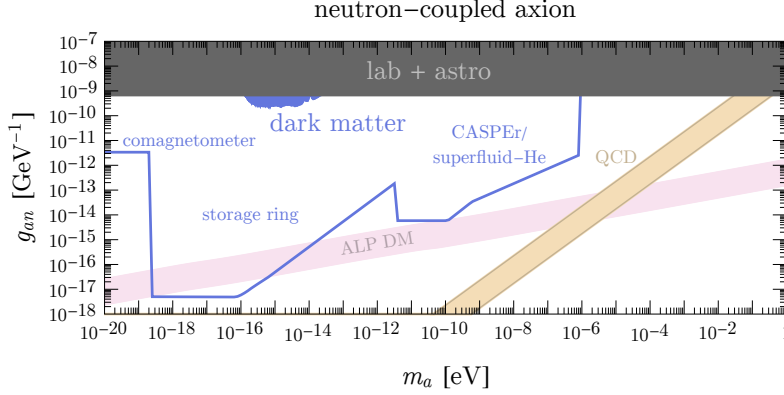
neutron−coupled axion

Figure 4

As in Fig. 1, but for neutron-coupled axions (Eq. 18 with $f = n$), in the parameter space spanned by the axion-neutron coupling g_{an} and the axion mass m_a. The orange band denotes the range of couplings for the DFSZ QCD axion. For hadronic QCD axions, such as in the KSVZ model, recent estimates are consistent with $g_{an} = 0$ (33).

3.3. Fermion Spin

Axion dark matter may also couple to Standard Model fermions $f = n, e, \ldots$, as in the last term of Eq. 1, which we rewrite here as[5]

$$\mathcal{L} \supset g_{af} \left(\partial_\mu a\right) \bar{\psi} \gamma^\mu \gamma^5 \psi \ , \qquad 18.$$

where $g_{af} \propto 1/f_a$. At low-energies, Eq. 18 gives rise to the following nonrelativistic single-particle Hamiltonian for f (123),

$$H \supset -g_{af} \left(\nabla a\right) \cdot \boldsymbol{\sigma} - \left(g_{af}/m_f\right) \left(\partial_t a\right) \boldsymbol{\sigma} \cdot \boldsymbol{\pi} \ , \qquad 19.$$

where $\boldsymbol{\pi} = \mathbf{p} - q_f \boldsymbol{A}$ is the mechanical momentum of the fermion with charge q_f, $\mathbf{p} = -i\nabla$ is the canonical momentum, and $\boldsymbol{A}$ the electromagnetic vector potential. The first and second terms of Eq. 19 are referred to as the "axion wind" and "axioelectric" terms. Their effect on Standard Model fermions can be deduced by working out the modifications to the fermion's equation of motion via Ehrenfest's theorem. Note that for the axion wind term, ∇a couples to the fermion's spin analogous to a magnetic field, whereas for the axioelectric term, $\left(\partial_t a\right) \boldsymbol{\sigma}$ couples to the fermion's momentum analogous to a vector potential.

As a result, the dominant effect of fermion-coupled axion dark matter is to act with a torque or force on fermion spins, which can be phrased in terms of an effective axion-wind magnetic field and axioelectric electric field, respectively,

$$\boldsymbol{B}_{\text{eff}} = \frac{g_{af}}{\mu_f} \nabla a \ , \quad \boldsymbol{E}_{\text{eff}} = -\frac{g_{af}}{q_f} \frac{d}{dt} \left(\dot{a} \langle \boldsymbol{\sigma} \rangle\right) \ , \qquad 20.$$

where μ_f is the Bohr or nuclear magneton for leptons or nucleons (123). For typical experimental setups in which $d\langle \boldsymbol{\sigma} \rangle/dt = 0$, $\boldsymbol{E}_{\text{eff}} \propto \ddot{a}$ decouples more rapidly at small axion masses,

---

[5]Although not considered in this review, it is also possible that the axion couples *off-diagonally* to the various fermion generations (120, 121, 122).
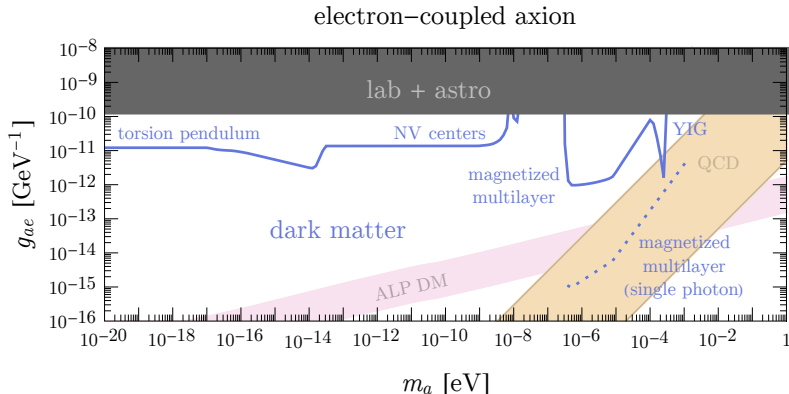
Figure 5

As in Fig. 1, but for electron-coupled axions (Eq. 18 with $f = e$), in the parameter space spanned by the axion-electron coupling g_{ae} and the axion mass m_a. The orange band denotes the range of couplings for the canonical QCD axion. The dotted blue line shows the maximum possible reach of a magnetized multilayer setup given noise-free detection of single photons (123).

such that $\boldsymbol{B}_{\text{eff}}$ leads to larger signals at low m_a. Existing limits and projected sensitivities are shown for the axion-neutron coupling and axion-electron coupling in Figs. 4 and 5.

Let us first focus on experimental schemes to detect the axion wind term. The effective magnetic field B_{eff} causes spins (nucleons or electrons, depending on the fermion coupled to the axion) to precess about ∇a, which is set by the direction of the dark matter wind $\mathbf{v}_{\text{DM}}$. Nuclear spins are best suited for low-frequency interactions, since they tend to be well-shielded from external degrees of freedom and their corresponding Larmor frequency is suppressed by the nucleon mass. Indeed, at sub-μeV frequencies, many precision magnetometry techniques may be immediately repurposed as an axion search, including spin-polarized torsion pendulums (124, 125), nuclear magnetic resonance experiments (126, 125, 127, 128), comagnetometers (129, 130, 131, 132), and hybrid spin resonance systems (133). Recently, there have also been proposals involving alternative techniques such as spin precession in storage rings (134, 135, 136), superfluid ^{3}He in both the A phase (137) and B phase (138, 139), and nitrogen vacancy centers (140).

For $m_a \gtrsim 1\,\mu$eV, the axion wind can couple to electron spin-excitations with larger characteristic energy. Such examples include spin-flip transitions in atoms (141) and in-medium magnon excitations (111). Since collective spin-excitations source electromagnetic fields, the most well-defined readout scheme for magnons are electromagnetic ones. For instance, certain experiments employ electromagnetic readout by placing an electron spin-polarized sample in a cavity, mixing the magnon and cavity modes (142, 143, 144). In order to leverage the high-Q of RF cavities, these setups employ low-loss magnetic insulators, such as yttrium iron garnet (YIG). However, such detectors are typically limited in exposure due to the fact that YIG crystals are difficult to manufacture beyond the mm-scale. Alternatively, one could incorporate cheaper magnetic materials, such as polycrystalline spinel ferrites, which can be scaled up to a much larger volume at the cost of increased loss. In this case, dielectric layers analogous to the MADMAX experiment discussed in Sec. 3.1.3, can be utilized, but to be sensitive to the axion-electron coupling, the dielectric needs to consist of

magnetic material. Such a setup, referred to as a "magnetized multilayer," was proposed in Ref. (123), involving sensitive photon detectors to probe unexplored parameter space at $\gtrsim$ GHz frequencies. More generally, for most experimental setups targeting the axion wind term, the total axion absorption power is governed by the *magnetic* energy-loss function, $P_{\text{sig}} \propto \mathbf{v}_{\text{DM}} \cdot \text{Im}(-\hat{\boldsymbol{\mu}}^{-1}) \cdot \mathbf{v}_{\text{DM}}$, where $\hat{\boldsymbol{\mu}}$ is the contribution of the spin of the fermion f to the medium's permeability tensor (i.e., for electrons this is the usual magnetic permeability) evaluated at the angular frequency m_a (123). Thus, the dissipative part of the target permeability completely determines the inclusive dark matter absorption rate.

Compared to the axion wind, the possible observables arising from the axioelectric term have not been as closely examined. Most effects can be understood from the corresponding effective electric field $\boldsymbol{E}_{\text{eff}}$, which acts as a force aligned along the spin of the fermion (123). For instance, for electron-coupled axions, the axioelectric term can induce modifications to atomic energy levels, although such effects are typically higher order in the electromagnetic fine-structure constant (123). $\boldsymbol{E}_{\text{eff}}$ can also acts as a bulk mechanical force in spin-polarized material, drive electronic excitations in molecules (145), superconductors (146), semiconductors (147), and materials hosting optical phonons (148), as well as induce polarization currents in dielectric stack experiments employing electron-polarized materials (123).

4. Producing and Detecting New Particles in the Lab

In Sec. 3, we focused on experiments searching for galactic dark matter present in the laboratory. Using the same interactions enumerated in Sec. 2, we may also produce the axion or dark photon fields in the laboratory, and subsequently reconvert them to detectable laboratory fields or forces. Such "light-shining-through-wall" experiments are generally more difficult than dark matter experiments because production and detection requires additional powers of small couplings. On the other hand, light-shining-through-wall experiments do not rely on dark matter being present in the lab, and are thus a powerful probe of *any* axion or dark photon in the Lagrangian of the universe, independent of any astrophysical uncertainties. As with dark matter experiments, the most straightforward detection strategies are electromagnetic, with new technologies recently providing vastly improved sensitivities. Axions may also lead to spin-dependent forces which can be detected with precision magnetometry and mechanical sensing.

4.1. Electromagnetic

Light-shining-through-wall experiments aim to both create and detect new particles, such as electromagnetically-coupled axions or dark photons. After first being sourced by the "emitter" (a region of strong electric E_{em} and/or magnetic B_{em} fields), these particles then propagate into a quiet shielded "receiver" region, in which they can excite small signal electromagnetic fields. The degree to which axions or dark photons are sourced by the emitter can be determined from their equations of motion, which are, respectively

$$(\partial^2 + m_a^2)\, a = g_{a\gamma\gamma}\, \boldsymbol{E} \cdot \boldsymbol{B} \qquad\qquad 21.$$

$$\left(\partial^2 + \frac{m_{A'}^2}{1 - \epsilon^2}\right) A_{\text{inv}}^\mu = -\frac{\epsilon\, m_{A'}^2}{1 - \epsilon^2}\, A^\mu\,, \qquad\qquad 22.$$

where on the left-hand side of Eq. 22 we have worked in the basis introduced above Eq. 14. From this, we see that axions are sourced by regions in which an electric *and* magnetic field

are aligned, whereas dark photon fields can be produced from either electric or magnetic fields. Regardless, the ideal emitter involves fields driven to high intensity, which can be achieved through the use of, e.g., optical or RF cavities. Furthermore, from the form of the effective currents in Eqs. 13 and 14, detecting the emitted axions requires an additional magnetic field $B_{\rm rec}$ in the receiver, whereas detection of emitted dark photons does not.

The figure of merit for these experiments is the probability for photons to convert into an axion or dark photon and then reconvert back into photons in the receiver. In optimal cavity setups operating at frequencies $\omega_{\rm exp}$ much greater than the axion or dark photon mass, the conversion probability is typically of the form

$$
P_{\gamma_{\rm em} \to \gamma_{\rm rec}} \sim
\begin{cases}
\left(g_{a\gamma\gamma} \sqrt{B_{\rm em}\, B_{\rm rec}}\, L_{\rm exp} \right)^4 & \text{(axion)} \\
\left(\epsilon\, m_{A'}/\omega_{\rm exp} \right)^4 & \text{(dark photon) ,}
\end{cases}
\qquad 23.
$$

where $L_{\rm exp}$ is an experimentally-dependent length scale, dictated by the size of the emitter and receiver and the distance separating them.In both cases, finesse and/or quality factors can further boost the power in the receiver cavity. A key difference between axion and dark photon experiments is the existence of the longitudinal mode of the dark photon, which can have a parametrically large effect on the signal, depending on the geometry of the experiment. As highlighted in Ref. (63), to obtain the $m_{A'}^4$ scaling in Eq. 23, the emitter and receiver cavities must be aligned with the direction of $\boldsymbol{E}_{\rm em}$; instead, if the receiver cavity is off-axis, then $P_{\rm conv} \propto m_{A'}^8$, which severely suppresses the signal rate for low-mass ($m_{A'} \ll \omega_{\rm exp}$) dark photons.

The strongest laboratory-based limits on dark photons come from the Dark SRF experiment (149), which utilizes 1.3 GHz emitter and receiver SRF cavities arranged coaxially to enhance sensitivity to the dark photon's longitudinal polarization. Both cavities have large intrinsic quality factors, $Q_{\rm int} \gtrsim 10^{10}$, a significant improvement over previous microwave cavity experiments with $Q \lesssim 10^4$ (150, 151). A first pathfinder run using $E_{\rm em} = 6.2$ MV/m and a total data-taking time of a few hours observed no excess power in the receiver cavity above thermal noise (following rejection of a peak also observed when the emitter cavity was off), and set a limit of $\epsilon \lesssim 1.6 \times 10^{-9} \times (5~\mu{\rm eV}/m_{A'})$ for $m_{A'} \lesssim 5~\mu{\rm eV}$. This was the first demonstration of high-Q SRF cavities for dark photon detection, including the required temperature and frequency stability. However, the sensitivity of this run was limited by an unwanted frequency offset between the emitter and receiver cavities. Future longer runs of the experiment with better frequency matching and larger $E_{\rm em}$ are expected to significantly improve the sensitivity.

For larger masses, i.e., when $m_a, m_{A'} \gg \omega_{\rm exp}$, axions and dark photons can only be sourced off-shell, corresponding to the production of evanescent fields that fall off exponentially within a Compton wavelength from the emitter. For light-shining-through-wall experiments whose emitter and receiver regions are separated by more than $\sim \omega_{\rm exp}^{-1}$, such signals are exponentially suppressed. This is the case for, e.g., Dark SRF, which has limited sensitivity to masses above GHz $\sim \mu{\rm eV}$. To get around this, Ref. (152) proposed using the *same* cavity as both source and receiver by simultaneously pumping two modes, which could offer better sensitivity at large axion masses, but likely suffers from a large irreducible background of nonlinear harmonic generation in the superconducting walls (153) (which may nonetheless be of some intrinsic interest to condensed matter physicists). However, for masses $\lesssim 1$ eV, the Compton wavelength is still much larger than the electromagnetic penetration depth in superconducting material ~ 50 nm. As a result, the emitter and receiver cavities can be separated by much less than a Compton wavelength while

also maintaining efficient shielding. Such light-shining-through-*thin*-wall (LSthinW) experiments were recently proposed in Ref. (64), which showed that setups analogous to Dark SRF could achieve sensitivity to unexplored dark photon parameter space for masses as large as $m_{A'} \sim \text{few} \times 10$ meV.

The strongest purely laboratory-based axion limits are expected to come from the ALPS II experiment (154), which consists of 1064 nm light propagating through a string of twelve 5.3 T magnets in the source region, followed by a similar configuration in the receiver region, for a total of $B_0 L_B = 560$ T m on each side. Mode-matched optical cavities are used to boost both source and receiver power, yielding an expected sensitivity to a conversion probability of $P_{\gamma_{\text{em}} \to \gamma_{\text{rec}}} \sim 10^{-25}$, i.e., a few photons per day with 40 W of source power. Two complementary detection strategies are envisioned for such weak signals: heterodyne detection by mixing the signal field with a strong local oscillator and performing single-photon counting at the beat frequency, followed by direct measurement of the signal photons with transition-edge sensors at an expected dark rate of 6.9×10^{-6} Hz. The first science-run data was collected in 2023, setting limits of $g_{a\gamma\gamma} \lesssim 6 \times 10^{-10}$ GeV^{-1}, and design sensitivity is expected to be achieved by 2025, with an expected sensitivity to $g_{a\gamma\gamma}$ of 2×10^{-11} GeV^{-1}. One may also envision using SRF cavities as source and receiver cavities (152, 155, 156, 157), with similar projected sensitivities as ALPS II but with different noise considerations.

Finally, we briefly mention helioscope experiments, which aim to detect axions produced from the Sun by converting them to keV X-ray photons with a spectrum determined by the solar temperature. The setup works similarly to ALPS II but without the source cavity, and thus the conversion probability is $(g_{a\gamma\gamma} B_{\text{rec}} L_{\text{exp}})^2$ for $m_a \ll$ keV. CAST (158), which consists of a 9 T LHC dipole magnet on a rotating mount to follow the direction of the Sun, completed data-taking in 2015 and set the strongest laboratory limits of $g_{a\gamma\gamma} < 6.6 \times 10^{-11}$ GeV^{-1} over many orders of magnitude in axion mass, which have persisted for almost a decade. The IAXO pathfinder (159) has implemented a new conversion gas to slightly improve sensitivity in the high-mass region, improving on a similar strategy used by CAST; by tuning the gas pressure, the plasma frequency can be tuned to match the axion mass, which makes the axion-to-photon conversion coherent over the length L_{exp} (analogous to the plasma haloscopes discussed in Sec. 3.1.3).

4.2. CP-violating couplings and axion-mediated forces

Recently, there has been interest in pursuing more exotic couplings, such as when axions possess interactions with Standard Model operators that are instead *even* under parity and time-reversal. As mentioned at the end of Sec. 3.2, this typically arises at higher order in the axion field, i.e., $\sim \mathcal{O}(a^2/f_a^2)$. This is indeed the case for minimal models of the QCD axion. To see this, note that the total effective QCD theta angle is $\theta_{\text{tot}} = \bar{\theta} + \langle a \rangle / f_a + a / f_a$, where $\bar{\theta}$ is the bare value, $\langle a \rangle$ is the axion vacuum expectation value, and a is the fluctuation around this value (e.g., in the case of dark matter $a/f_a = \theta_a$ in Eq. 17). When the only source of parity and time-reversal violation is $\bar{\theta} \neq 0$, the energetic minimum is achieved at $\langle a \rangle / f_a = -\bar{\theta}$, such that $\theta_{\text{tot}} = a/f_a$ (160). Since parity and time-reversal symmetric operators couple only to the square of θ_{tot} at leading order, the same is true for a/f_a.

However, if there are additional sources of parity and time-reversal violation beyond $\bar{\theta}$, these can induce $\langle a \rangle / f_a \neq -\bar{\theta}$, such that $\theta_{\text{tot}} = \theta_{\text{eff}} + a/f_a$, where $\theta_{\text{eff}} \equiv \bar{\theta} + \langle a \rangle / f_a \neq 0$. While the Standard Model contribution to θ_{eff} is experimentally negligible, additional new physics may lead to values that saturate the current experimental limit of $\theta_{\text{eff}} \lesssim 10^{-10}$.

Scalar interactions controlled by θ_{tot}^2 therefore involve the cross product $\theta_{\mathrm{eff}} \times (a/f_a)$. For example, such considerations imply the existence of scalar couplings between the axion and Standard Model fermions parametrically of the form $\mathcal{L} \sim \theta_{\mathrm{eff}} \, (m_f/f_a) \, a \, \bar{\psi}\psi$, where m_f is the mass of the fermion (161) (see also, e.g., Refs. (162, 163) for recent discussions of these points). In this case, the axion can be sourced by matter density alone, and then may be detected with, e.g., its standard coupling to electromagnetism or spin. Various schemes along these lines have been proposed using spin probes for axions produced by laboratory sources (164) or the Earth (165, 166).

In the case of laboratory sources, one physical effect is that of a spin-dependent axion-mediated force (164), where a source mass creates an effective magnetic field which can in turn be detected with NMR techniques, like those reviewed in Sec. 3.3. The ARIADNE collaboration (167, 168) aims to use tungsten as the source mass and polarized ^{3}He as the detection medium, with projected sensitivity to the QCD axion in the $(10^{-3} - 10^{-5})$ eV mass range.

5. Looking Forward

As we have surveyed in this review article, the creativity and interdisciplinarity exhibited by the axion and dark photon community is enormous, with dozens of new experiments proposed in the decade since the last such review (11). Without discounting the enormous effort represented by this cumulative body of work, no discovery of axion or dark photon dark matter has yet been made. In that light, it is worth evaluating the progress of experiments over the past decade in an effort to identify which regimes of parameter space still remain unprobed, which technological aspects have been bottlenecks to progress, and where effort might best be spent to fully probe the best-motivated dark matter models.

The most rapid progress has been made in experiments searching for the axion electromagnetic coupling. While several new searches have obtained sensitivity in narrow frequency ranges, often dipping down into the canonical QCD axion parameter space, a broad program covering the QCD axion over several decades of mass remains an important goal for the future. For cavity searches, the principal technological challenge is the $B_0^4 \, V_{\mathrm{exp}}^2$ scaling of the scan rate in Eq. 16. For a single-mode haloscope, achieving DFSZ sensitivity over the $(1 - 10)$ GHz range with current B-field strengths and $Q_L \sim 10^6$ would take 20,000 years of scanning at 100% livetime (169). The technology we described in this review – including squeezing and photon counting to push beyond the standard quantum limit, and SRF cavities with extremely large Q_L, both of which have been experimentally demonstrated in the past decade – may reduce this daunting task to a more manageable level. However, the most rapid improvements may come with development of high-field magnets, which is strongly synergistic with the fusion energy program (170).

We further emphasize that the ρ_{DM}^2 scaling of the scan rate from Eq. 16 (given our uncertainty on the dark matter density and substructure) implies that a comprehensive search strategy must include probing couplings *below* those corresponding to the "standard" value of $\rho_{\mathrm{DM}} \simeq 0.45$ GeV/cm^3, a value which is primarily adopted for convenience in comparing experiments rather than a quantity of intrinsic physical significance.

At sub-GHz frequencies, initial development is underway to manufacture tunable lumped-element circuits and high-Q SRF cavities with nearly degenerate modes. However, the importance of noise sources that are more prevalent in this regime, such as low-frequency vibrational noise (171), remains to be seen. If such noise sources can be mitigated, these

approaches provide a plausible path to QCD axion detection for masses corresponding to GUT-scale decay constants. At high frequencies, SNSPDs have demonstrated excellent performance in the optical and near-infrared frequency range, but further work is needed to demonstrate a viable path toward QCD axion detection in the "THz gap," which may benefit from the synergy with development of single-photon THz sensors for astrophysics applications (172, 173).

By contrast, the parameter space for spin-coupled axion dark matter looks much the same as it did a decade ago. The only experiments whose exclusion limits dip beyond the long-standing neutron star cooling constraints operate in a broadband mode at low frequencies, one of which actually used archival data first taken in 2009 for other purposes (132). The situation for the defining gluon coupling of the QCD axion is perhaps even starker, with broadband experiments only able to probe axions below 100 Hz, and resonant experiments limited to narrow "fingers" of parameter space which do not yet improve upon SN1987A constraints. As outlined in Sec. 3.2, the gluon coupling can be probed with electromagnetic sensors coupled to nuclear spin-polarized material; however, such strategies are typically hindered by the fact that the QCD axion generates an EDM current much smaller than the effective current from its photon coupling, $J_{\mathrm{EDM}}/J_{a\gamma} \lesssim 10^{-3} \times (10 \mathrm{~T}/B_0)$ (112). New and creative experimental approaches are thus needed to fully explore these well-motivated regions of parameter space.

The search for dark photons will benefit from the continued development of axion experiments, as many of the projections shown in Fig. 2 correspond to axion experiments without the direct use of the magnetic field. While there is no sharp target in mass-coupling space analogous to the QCD axion, we encourage the experimental community to continue pursuing these searches. In particular, we encourage axion experiments to publish dedicated dark photon searches. With regards to light-shining-through-wall experiments, Dark SRF clearly demonstrates the benefits of high-Q SRF cavities for dark photon detection, and ALPS II should soon achieve its design sensitivity for axions.

To close, we commend once again the combined creativity and efforts of theorists and experimentalists to vastly expand the suite of experiments searching for the axion and dark photon. New technologies have been brought to bear on this problem over the past decade, many of which have shown the potential for technology transfer to physics from fields as diverse as microwave engineering, precision magnetometry, and quantum sensing. While a discovery of new physics is never assured, the field has always progressed by looking in new places, and we look forward to the new and insightful approaches to be proposed and implemented in the decade to come.

DISCLOSURE STATEMENT

ACKNOWLEDGMENTS

LITERATURE CITED

1. G. Jungman, M. Kamionkowski and K. Griest, *Supersymmetric dark matter*, *Phys. Rept.* **267** (1996) 195 [`hep-ph/9506380`].

2. G. Bertone and D. Hooper, *History of dark matter*, *Rev. Mod. Phys.* **90** (2018) 045002 [`1605.04909`].

3. M. Cirelli, A. Strumia and J. Zupan, *Dark Matter*, `2406.01705`.

4. J.N. Butler et al., *Report of the 2021 U.S. Community Study on the Future of Particle Physics (Snowmass 2021)*, .

5. P. Svrcek and E. Witten, *Axions In String Theory*, *JHEP* **06** (2006) 051 [`hep-th/0605206`].

6. A. Arvanitaki, S. Dimopoulos, S. Dubovsky, N. Kaloper and J. March-Russell, *String Axiverse*, *Phys. Rev. D* **81** (2010) 123530 [`0905.4720`].

7. J. Halverson and P. Langacker, *TASI Lectures on Remnants from the String Landscape*, *PoS* **TASI2017** (2018) 019 [`1801.03503`].

8. Y. Hochberg, Y.F. Kahn, R.K. Leane, S. Rajendran, K. Van Tilburg, T.-T. Yu et al., *New approaches to dark matter detection*, *Nature Rev. Phys.* **4** (2022) 637.

9. R. Essig, Y. Kahn, S. Knapen, A. Ringwald and N. Toro, *Snowmass2021 Theory Frontier: Theory Meets the Lab*, in *Snowmass 2021*, 3, 2022 [`2203.10089`].

10. S.J. Asztalos, L.J. Rosenberg, K. van Bibber, P. Sikivie and K. Zioutas, *Searches for astrophysical and cosmological axions*, *Ann. Rev. Nucl. Part. Sci.* **56** (2006) 293.

11. P.W. Graham, I.G. Irastorza, S.K. Lamoreaux, A. Lindner and K.A. van Bibber, *Experimental Searches for the Axion and Axion-Like Particles*, *Ann. Rev. Nucl. Part. Sci.* **65** (2015) 485 [`1602.00039`].

12. M. Baryakhtar et al., *Dark Matter In Extreme Astrophysical Environments*, in *Snowmass 2021*, 3, 2022 [`2203.07984`].

13. C. Dvorkin et al., *The Physics of Light Relics*, in *Snowmass 2021*, 3, 2022 [`2203.07943`].

14. A. Boveia et al., *Snowmass 2021 Cross Frontier Report: Dark Matter Complementarity (Extended Version)*, `2210.01770`.

15. A. Drlica-Wagner et al., *Report of the Topical Group on Cosmic Probes of Dark Matter for Snowmass 2021*, `2209.08215`.

16. J. Alvey, N. Sabti, V. Tiki, D. Blas, K. Bondarenko, A. Boyarsky et al., *New constraints on the mass of fermionic dark matter from dwarf spheroidal galaxies*, *Mon. Not. Roy. Astron. Soc.* **501** (2021) 1188 [`2010.03572`].

17. N. Dalal and A. Kravtsov, *Excluding fuzzy dark matter with sizes and stellar kinematics of ultrafaint dwarf galaxies*, *Phys. Rev. D* **106** (2022) 063517 [`2203.05750`].

18. T. Zimmermann, J. Alvey, D.J.E. Marsh, M. Fairbairn and J.I. Read, *Dwarf galaxies imply dark matter is heavier than $\mathbf{2.2 \times 10^{-21}}$ eV*, `2405.20374`.

19. S. Weinberg, *Feynman Rules for Any Spin. 2. Massless Particles*, *Phys. Rev.* **134** (1964) B882.

20. S. Weinberg, *Photons and Gravitons in S-Matrix Theory: Derivation of Charge Conservation and Equality of Gravitational and Inertial Mass*, Phys. Rev. **135** (1964) B1049.

21. S. Weinberg, *Photons and gravitons in perturbation theory: Derivation of Maxwell's and Einstein's equations*, Phys. Rev. **138** (1965) B988.

22. S. Weinberg and E. Witten, *Limits on Massless Particles*, Phys. Lett. B **96** (1980) 59.

23. N. Craig, *Naturalness: past, present, and future*, Eur. Phys. J. C **83** (2023) 825 [2205.05708].

24. R.D. Peccei and H.R. Quinn, *CP Conservation in the Presence of Instantons*, Phys. Rev. Lett. **38** (1977) 1440.

25. J.A. Dror, R. Lasenby and M. Pospelov, *New constraints on light vectors coupled to anomalous currents*, Phys. Rev. Lett. **119** (2017) 141803 [1705.06726].

26. J.A. Dror, R. Lasenby and M. Pospelov, *Dark forces coupled to nonconserved currents*, Phys. Rev. D **96** (2017) 075036 [1707.01503].

27. M. Fabbrichesi, E. Gabrielli and G. Lanfranchi, *The Dark Photon*, 2005.01515.

28. A. Caputo, A.J. Millar, C.A.J. O'Hare and E. Vitagliano, *Dark photon limits: A handbook*, Phys. Rev. D **104** (2021) 095029 [2105.04565].

29. B. Holdom, *Two U(1)'s and Epsilon Charge Shifts*, Phys. Lett. B **166** (1986) 196.

30. R.D. Peccei and H.R. Quinn, *Constraints Imposed by CP Conservation in the Presence of Instantons*, Phys. Rev. D **16** (1977) 1791.

31. S. Weinberg, *A New Light Boson?*, Phys. Rev. Lett. **40** (1978) 223.

32. F. Wilczek, *Problem of Strong P and T Invariance in the Presence of Instantons*, Phys. Rev. Lett. **40** (1978) 279.

33. G. Grilli di Cortona, E. Hardy, J. Pardo Vega and G. Villadoro, *The QCD axion, precisely*, JHEP **01** (2016) 034 [1511.02867].

34. C.A. Baker et al., *An Improved experimental limit on the electric dipole moment of the neutron*, Phys. Rev. Lett. **97** (2006) 131801 [hep-ex/0602020].

35. C. Abel et al., *Measurement of the Permanent Electric Dipole Moment of the Neutron*, Phys. Rev. Lett. **124** (2020) 081803 [2001.11966].

36. A. Hook, *Solving the Hierarchy Problem Discretely*, Phys. Rev. Lett. **120** (2018) 261802 [1802.10093].

37. L. Di Luzio, B. Gavela, P. Quilez and A. Ringwald, *An even lighter QCD axion*, JHEP **05** (2021) 184 [2102.00012].

38. L. Di Luzio, B. Gavela, P. Quilez and A. Ringwald, *Dark matter from an even lighter QCD axion: trapped misalignment*, JCAP **10** (2021) 001 [2102.01082].

39. J.E. Kim, *Weak Interaction Singlet and Strong CP Invariance*, Phys. Rev. Lett. **43** (1979) 103.

40. M.A. Shifman, A.I. Vainshtein and V.I. Zakharov, *Can Confinement Ensure Natural CP Invariance of Strong Interactions?*, Nucl. Phys. B **166** (1980) 493.

41. A.R. Zhitnitsky, *On Possible Suppression of the Axion Hadron Interactions. (In Russian)*, Sov. J. Nucl. Phys. **31** (1980) 260.

42. M. Dine, W. Fischler and M. Srednicki, *A Simple Solution to the Strong CP Problem with a Harmless Axion*, Phys. Lett. B **104** (1981) 199.

43. C. Cheung, J.T. Ruderman, L.-T. Wang and I. Yavin, *Kinetic Mixing as the Origin of Light Dark Scales*, Phys. Rev. D **80** (2009) 035008 [0902.3246].

44. T. Gherghetta, J. Kersten, K. Olive and M. Pospelov, *Evaluating the price of tiny kinetic mixing*, Phys. Rev. D **100** (2019) 095001 [1909.00696].

45. N. Arkani-Hamed and N. Weiner, *LHC Signals for a SuperUnified Theory of Dark Matter*, JHEP **12** (2008) 104 [0810.0714].

46. N. Blinov, M.J. Dolan, P. Draper and J. Kozaczuk, *Dark matter targets for axionlike particle searches*, Phys. Rev. D **100** (2019) 015049 [1905.06952].

47. C.A.J. O'Hare, *Cosmology of axion dark matter*, PoS **COSMICWISPers** (2024) 040

[2403.17697].

48. P.F. de Salas and A. Widmark, *Dark matter local density determination: recent observations and future prospects*, Rept. Prog. Phys. **84** (2021) 104901 [2012.11477].

49. C.J. Hogan and M.J. Rees, *AXION MINICLUSTERS*, Phys. Lett. B **205** (1988) 228.

50. E.W. Kolb and I.I. Tkachev, *Large amplitude isothermal fluctuations and high density dark matter clumps*, Phys. Rev. D **50** (1994) 769 [astro-ph/9403011].

51. E.W. Kolb and I.I. Tkachev, *Femtolensing and picolensing by axion miniclusters*, Astrophys. J. Lett. **460** (1996) L25 [astro-ph/9510043].

52. A. Arvanitaki, S. Dimopoulos, M. Galanis, L. Lehner, J.O. Thompson and K. Van Tilburg, *Large-misalignment mechanism for the formation of compact axion structures: Signatures from the QCD axion to fuzzy dark matter*, Phys. Rev. D **101** (2020) 083014 [1909.11665].

53. A. Derevianko, *Detecting dark-matter waves with a network of precision-measurement tools*, Phys. Rev. A **97** (2018) 042506 [1605.09717].

54. A. Hook, *TASI Lectures on the Strong CP Problem and Axions*, PoS **TASI2018** (2019) 004 [1812.02669].

55. J.-D. Bernal, R.B. Petery, K.J. Joven and S. Singh, *Characterizing the quantum properties of ultralight dark matter – an open quantum systems approach*, 2406.10412.

56. D.Y. Cheong, N.L. Rodd and L.-T. Wang, *A Quantum Description of Wave Dark Matter*, 2408.04696.

57. S. Knirck, A.J. Millar, C.A.J. O'Hare, J. Redondo and F.D. Steffen, *Directional axion detection*, JCAP **11** (2018) 051 [1806.05927].

58. M. Lisanti, M. Moschella and W. Terrano, *Stochastic properties of ultralight scalar field gradients*, Phys. Rev. D **104** (2021) 055037 [2107.10260].

59. J.W. Foster, Y. Kahn, R. Nguyen, N.L. Rodd and B.R. Safdi, *Dark Matter Interferometry*, Phys. Rev. D **103** (2021) 076018 [2009.14201].

60. S. De Panfilis, A.C. Melissinos, B.E. Moskowitz, J.T. Rogers, Y.K. Semertzidis, W. Wuensch et al., *Limits on the Abundance and Coupling of Cosmic Axions at 4.5-Microev < m(a) < 5.0-Microev*, Phys. Rev. Lett. **59** (1987) 839.

61. W. Wuensch, S. De Panfilis-Wuensch, Y.K. Semertzidis, J.T. Rogers, A.C. Melissinos, H.J. Halama et al., *Results of a Laboratory Search for Cosmic Axions and Other Weakly Coupled Light Particles*, Phys. Rev. D **40** (1989) 3153.

62. C. Hagmann, P. Sikivie, N.S. Sullivan and D.B. Tanner, *Results from a search for cosmic axions*, Phys. Rev. D **42** (1990) 1297.

63. P.W. Graham, J. Mardon, S. Rajendran and Y. Zhao, *Parametrically enhanced hidden photon search*, Phys. Rev. D **90** (2014) 075017 [1407.4806].

64. A. Berlin, R. Harnik and R. Janish, *Light Shining Through a Thin Wall: Evanescent Hidden Photon Detection*, 2303.00014.

65. A. Berlin, J.A. Dror, X. Gan and J.T. Ruderman, *Millicharged relics reveal massless dark photons*, JHEP **05** (2023) 046 [2211.05139].

66. A. Berlin, R. Tito D'Agnolo, S.A.R. Ellis and J.I. Radkovski, *Signals of millicharged dark matter in light-shining-through-wall experiments*, JHEP **08** (2023) 017 [2305.05684].

67. J.N. Benabou, J.W. Foster, Y. Kahn, B.R. Safdi and C.P. Salemi, *Lumped-element axion dark matter detection beyond the magnetoquasistatic limit*, Phys. Rev. D **108** (2023) 035009 [2211.00008].

68. S. Chaudhuri, K. Irwin, P.W. Graham and J. Mardon, *Optimal Impedance Matching and Quantum Limits of Electromagnetic Axion and Hidden-Photon Dark Matter Searches*, 1803.01627.

69. A. Berlin, R.T. D'Agnolo, S.A.R. Ellis, C. Nantista, J. Neilson, P. Schuster et al., *Axion Dark Matter Detection by Superconducting Resonant Frequency Conversion*, JHEP **07** (2020) 088 [1912.11048].

70. R. Cervantes et al., *Deepest sensitivity to wavelike dark photon dark matter with*

superconducting radio frequency cavities, *Phys. Rev. D* **110** (2024) 043022 [2208.03183].

71. ADMX COLLABORATION collaboration, *Search for invisible axion dark matter with the axion dark matter experiment*, *Phys. Rev. Lett.* **120** (2018) 151301.

72. ADMX COLLABORATION collaboration, *Extended search for the invisible axion with the axion dark matter experiment*, *Phys. Rev. Lett.* **124** (2020) 101303.

73. ADMX COLLABORATION collaboration, *Search for invisible axion dark matter in the $3.3 - -4.2$ μeV mass range*, *Phys. Rev. Lett.* **127** (2021) 261803.

74. S. Ahn, J. Kim, B.I. Ivanov, O. Kwon, H. Byun, A.F. van Loo et al., *Extensive search for axion dark matter over 1 ghz with capp's main axion experiment*, *Phys. Rev. X* **14** (2024) 031023.

75. A. Romanenko, A. Grassellino, A.C. Crawford, D.A. Sergatskov and O. Melnychuk, *Ultra-high quality factors in superconducting niobium cavities in ambient magnetic fields up to 190 mG*, *Appl. Phys. Lett.* **105** (2014) 234103 [1410.7877].

76. S. Posen, M. Checchin, O.S. Melnychuk, T. Ring, I. Gonin and T. Khabiboulline, *High-Quality-Factor Superconducting Cavities in Tesla-Scale Magnetic Fields for Dark-Matter Searches*, *Phys. Rev. Applied* **20** (2023) 034004 [2201.10733].

77. D. Alesini et al., *Galactic axions search with a superconducting resonant cavity*, *Phys. Rev. D* **99** (2019) 101101 [1903.06547].

78. S. Belomestnykh et al., *Key directions for research and development of superconducting radio frequency cavities*, in *Snowmass 2021*, 4, 2022 [2204.01178].

79. H. Yoon, M. Ahn, B. Yang, Y. Lee, D. Kim, H. Park et al., *Axion haloscope using an 18 T high temperature superconducting magnet*, *Phys. Rev. D* **106** (2022) 092007 [2206.12271].

80. D. Ahn, O. Kwon, W. Chung, W. Jang, D. Lee, J. Lee et al., *Maintaining high Q-factor of superconducting $YBa_2Cu_3O_{7-x}$ microwave cavity in a high magnetic field*, 1904.05111.

81. D. Ahn, D. Youm, O. Kwon, W. Chung and Y.K. Semertzidis, *High Quality Factor High-Temperature Superconducting Microwave Cavity Development for the Dark Matter Axion Search in a Strong Magnetic Field*, 1902.04551.

82. DMRADIO collaboration, *Projected sensitivity of DMRadio-m3: A search for the QCD axion below 1 μeV*, *Phys. Rev. D* **106** (2022) 103008 [2204.13781].

83. N. Crisosto, P. Sikivie, N.S. Sullivan, D.B. Tanner, J. Yang and G. Rybka, *ADMX SLIC: Results from a Superconducting LC Circuit Investigating Cold Axions*, *Phys. Rev. Lett.* **124** (2020) 241101 [1911.05772].

84. DMRADIO collaboration, *Electromagnetic modeling and science reach of DMRadio-m^3*, 2302.14084.

85. C.P. Salemi et al., *Search for Low-Mass Axion Dark Matter with ABRACADABRA-10 cm*, *Phys. Rev. Lett.* **127** (2021) 081801 [2102.06722].

86. A.V. Gramolin, D. Aybas, D. Johnson, J. Adam and A.O. Sushkov, *Search for axion-like dark matter with ferromagnets*, *Nature Phys.* **17** (2021) 79 [2003.03348].

87. R. Lasenby, *Microwave cavity searches for low-frequency axion dark matter*, *Phys. Rev. D* **102** (2020) 015008 [1912.11056].

88. A. Berlin, R.T. D'Agnolo, S.A.R. Ellis and K. Zhou, *Heterodyne broadband detection of axion dark matter*, *Phys. Rev. D* **104** (2021) L111701 [2007.15656].

89. B. Giaccone et al., *Design of axion and axion dark matter searches based on ultra high Q SRF cavities*, 2207.11346.

90. S. Chaudhuri, K.D. Irwin, P.W. Graham and J. Mardon, *Optimal Electromagnetic Searches for Axion and Hidden-Photon Dark Matter*, 1904.05806.

91. S.E. Kuenstner et al., *Quantum metrology of low frequency electromagnetic modes with frequency upconverters*, 2210.05576.

92. W. DeRocco and A. Hook, *Axion interferometry*, *Phys. Rev. D* **98** (2018) 035021 [1802.07273].

93. H. Liu, B.D. Elwood, M. Evans and J. Thaler, *Searching for Axion Dark Matter with*

Birefringent Cavities, *Phys. Rev. D* **100** (2019) 023548 [`1809.01656`].

94. HAYSTAC collaboration, *A quantum-enhanced search for dark matter axions*, *Nature* **590** (2021) 238 [`2008.01853`].

95. HAYSTAC collaboration, *New results from HAYSTAC's phase II operation with a squeezed state receiver*, *Phys. Rev. D* **107** (2023) 072007 [`2301.09721`].

96. A.V. Dixit, S. Chakram, K. He, A. Agrawal, R.K. Naik, D.I. Schuster et al., *Searching for Dark Matter with a Superconducting Qubit*, *Phys. Rev. Lett.* **126** (2021) 141302 [`2008.12231`].

97. A. Agrawal, A.V. Dixit, T. Roy, S. Chakram, K. He, R.K. Naik et al., *Stimulated Emission of Signal Photons from Dark Matter Waves*, *Phys. Rev. Lett.* **132** (2024) 140801 [`2305.03700`].

98. M. Bal et al., *Systematic improvements in transmon qubit coherence enabled by niobium surface encapsulation*, *npj Quantum Inf.* **10** (2024) 43 [`2304.13257`].

99. https://www.snowmass21.org/docs/files/summaries/CF/SNOWMASS21-CF2_CF0_Andrew_Sonnenschein-093.pdf.

100. M. Lawson, A.J. Millar, M. Pancaldi, E. Vitagliano and F. Wilczek, *Tunable axion plasma haloscopes*, *Phys. Rev. Lett.* **123** (2019) 141802 [`1904.11872`].

101. M. Wooten, A. Droster, A. Kenany, D. Sun, S.M. Lewis and K. van Bibber, *Exploration of Wire Array Metamaterials for the Plasma Axion Haloscope*, *Annalen Phys.* **536** (2024) 2200479 [`2203.13945`].

102. MADMAX collaboration, *A new experimental approach to probe QCD axion dark matter in the mass range above 40 μeV*, *Eur. Phys. J. C* **79** (2019) 186 [`1901.07401`].

103. DALI collaboration, *Discovery prospects with the Dark-photons & Axion-like particles Interferometer*, *Phys. Rev. D* **109** (2024) 062002 [`2303.03997`].

104. MADMAX collaboration, *First search for dark photon dark matter with a MADMAX prototype*, 2408.02368.

105. M. Baryakhtar, J. Huang and R. Lasenby, *Axion and hidden photon dark matter detection with multilayer optical haloscopes*, *Phys. Rev. D* **98** (2018) 035006 [`1803.11455`].

106. J. Chiles et al., *New Constraints on Dark Photon Dark Matter with Superconducting Nanowire Detectors in an Optical Haloscope*, *Phys. Rev. Lett.* **128** (2022) 231802 [`2110.01582`].

107. L. Manenti et al., *Search for dark photons using a multilayer dielectric haloscope equipped with a single-photon avalanche diode*, *Phys. Rev. D* **105** (2022) 052010 [`2110.10497`].

108. BREAD collaboration, *Broadband Solenoidal Haloscope for Terahertz Axion Detection*, *Phys. Rev. Lett.* **128** (2022) 131801 [`2111.12103`].

109. B. Godfrey et al., *Search for dark photon dark matter: Dark E field radio pilot experiment*, *Phys. Rev. D* **104** (2021) 012013 [`2101.02805`].

110. A. Berlin and T. Trickle, *Absorption of Axion Dark Matter in a Magnetized Medium*, *Phys. Rev. Lett.* **132** (2024) 181801 [`2305.05681`].

111. A. Mitridate, T. Trickle, Z. Zhang and K.M. Zurek, *Detectability of Axion Dark Matter with Phonon Polaritons and Magnons*, *Phys. Rev. D* **102** (2020) 095005 [`2005.10256`].

112. A. Berlin and K. Zhou, *Discovering QCD-coupled axion dark matter with polarization haloscopes*, *Phys. Rev. D* **108** (2023) 035038 [`2209.12901`].

113. D. Budker, P.W. Graham, M. Ledbetter, S. Rajendran and A. Sushkov, *Proposal for a Cosmic Axion Spin Precession Experiment (CASPEr)*, *Phys. Rev. X* **4** (2014) 021030 [`1306.6089`].

114. D.F. Jackson Kimball et al., *Overview of the Cosmic Axion Spin Precession Experiment (CASPEr)*, *Springer Proc. Phys.* **245** (2020) 105 [`1711.08999`].

115. J.A. Dror, S. Gori, J.M. Leedom and N.L. Rodd, *Sensitivity of Spin-Precession Axion Experiments*, *Phys. Rev. Lett.* **130** (2023) 181801 [`2210.06481`].

116. A. Arvanitaki, A. Madden and K. Van Tilburg, *Piezoaxionic effect*, *Phys. Rev. D* **109** (2024) 072009 [`2112.11466`].

117. K. Blum, R.T. D'Agnolo, M. Lisanti and B.R. Safdi, *Constraining Axion Dark Matter with Big Bang Nucleosynthesis*, *Phys. Lett. B* **737** (2014) 30 [1401.6460].

118. H. Kim, A. Lenoci, G. Perez and W. Ratzinger, *Probing an ultralight QCD axion with electromagnetic quadratic interaction*, *Phys. Rev. D* **109** (2024) 015030 [2307.14962].

119. C. Beadle, S.A.R. Ellis, J. Quevillon and P.N. Hoa Vuong, *Quadratic coupling of the axion to photons*, *Phys. Rev. D* **110** (2024) 035019 [2307.10362].

120. F. Wilczek, *Axions and Family Symmetry Breaking*, *Phys. Rev. Lett.* **49** (1982) 1549.

121. F. Björkeroth, E.J. Chun and S.F. King, *Flavourful Axion Phenomenology*, *JHEP* **08** (2018) 117 [1806.00660].

122. J. Martin Camalich, M. Pospelov, P.N.H. Vuong, R. Ziegler and J. Zupan, *Quark Flavor Phenomenology of the QCD Axion*, *Phys. Rev. D* **102** (2020) 015023 [2002.04623].

123. A. Berlin, A.J. Millar, T. Trickle and K. Zhou, *Physical signatures of fermion-coupled axion dark matter*, *JHEP* **05** (2024) 314 [2312.11601].

124. W.A. Terrano, E.G. Adelberger, C.A. Hagedorn and B.R. Heckel, *Constraints on axionlike dark matter with masses down to 10^{-23} eV/c^2*, *Phys. Rev. Lett.* **122** (2019) 231301 [1902.04246].

125. P.W. Graham, D.E. Kaplan, J. Mardon, S. Rajendran, W.A. Terrano, L. Trahms et al., *Spin Precession Experiments for Light Axionic Dark Matter*, *Phys. Rev. D* **97** (2018) 055006 [1709.07852].

126. P.W. Graham and S. Rajendran, *New Observables for Direct Detection of Axion Dark Matter*, *Phys. Rev. D* **88** (2013) 035023 [1306.6088].

127. C. Abel et al., *Search for Axionlike Dark Matter through Nuclear Spin Precession in Electric and Magnetic Fields*, *Phys. Rev. X* **7** (2017) 041034 [1708.06367].

128. Z. Xu et al., *Constraining ultralight dark matter through an accelerated resonant search*, *Commun. Phys.* **7** (2024) 226 [2309.16600].

129. T. Wu et al., *Search for Axionlike Dark Matter with a Liquid-State Nuclear Spin Comagnetometer*, *Phys. Rev. Lett.* **122** (2019) 191302 [1901.10843].

130. NASDUCK collaboration, *New constraints on axion-like dark matter using a Floquet quantum detector*, *Sci. Adv.* **8** (2022) abl8919 [2105.04603].

131. NASDUCK collaboration, *Constraints on axion-like dark matter from a SERF comagnetometer*, *Nature Commun.* **14** (2023) 5784 [2209.13588].

132. J. Lee, M. Lisanti, W.A. Terrano and M. Romalis, *Laboratory Constraints on the Neutron-Spin Coupling of feV-Scale Axions*, *Phys. Rev. X* **13** (2023) 011050 [2209.03289].

133. K. Wei et al., *Dark matter search with a strongly-coupled hybrid spin system*, 2306.08039.

134. P.W. Graham, S. Hacıömeroğlu, D.E. Kaplan, Z. Omarov, S. Rajendran and Y.K. Semertzidis, *Storage ring probes of dark matter and dark energy*, *Phys. Rev. D* **103** (2021) 055010 [2005.11867].

135. R. Janish and H. Ramani, *Muon g-2 and EDM experiments as muonic dark matter detectors*, *Phys. Rev. D* **102** (2020) 115018 [2006.10069].

136. JEDI collaboration, *First Search for Axionlike Particles in a Storage Ring Using a Polarized Deuteron Beam*, *Phys. Rev. X* **13** (2023) 031004 [2208.07293].

137. S. Chigusa, D. Kondo, H. Murayama, R. Okabe and H. Sudo, *Axion detection via superfluid ^3He ferromagnetic phase and quantum measurement techniques*, 2309.09160.

138. C. Gao, W. Halperin, Y. Kahn, M. Nguyen, J. Schütte-Engel and J.W. Scott, *Axion Wind Detection with the Homogeneous Precession Domain of Superfluid Helium-3*, *Phys. Rev. Lett.* **129** (2022) 211801 [2208.14454].

139. J.W. Foster, C. Gao, W. Halperin, Y. Kahn, A. Mande, M. Nguyen et al., *The statistics and sensitivity of axion wind detection with the homogeneous precession domain of superfluid helium-3*, 2310.07791.

140. S. Chigusa, M. Hazumi, E.D. Herbschleb, N. Mizuochi and K. Nakayama, *Light Dark Matter Search with Nitrogen-Vacancy Centers in Diamonds*, 2302.12756.

141. P. Sikivie, *Axion Dark Matter Detection using Atomic Transitions*, Phys. Rev. Lett. **113** (2014) 201301 [1409.2806].

142. R. Barbieri, C. Braggio, G. Carugno, C.S. Gallo, A. Lombardi, A. Ortolan et al., *Searching for galactic axions through magnetized media: the QUAX proposal*, Phys. Dark Univ. **15** (2017) 135 [1606.02201].

143. QUAX collaboration, *Axion search with a quantum-limited ferromagnetic haloscope*, Phys. Rev. Lett. **124** (2020) 171801 [2001.08940].

144. T. Ikeda, A. Ito, K. Miuchi, J. Soda, H. Kurashige and Y. Shikano, *Axion search with quantum nondemolition detection of magnons*, Phys. Rev. D **105** (2022) 102004 [2102.08764].

145. A. Arvanitaki, S. Dimopoulos and K. Van Tilburg, *Resonant absorption of bosonic dark matter in molecules*, Phys. Rev. X **8** (2018) 041001 [1709.05354].

146. Y. Hochberg, T. Lin and K.M. Zurek, *Detecting Ultralight Bosonic Dark Matter via Absorption in Superconductors*, Phys. Rev. D **94** (2016) 015019 [1604.06800].

147. Y. Hochberg, T. Lin and K.M. Zurek, *Absorption of light dark matter in semiconductors*, Phys. Rev. D **95** (2017) 023013 [1608.01994].

148. A. Mitridate, T. Trickle, Z. Zhang and K.M. Zurek, *Dark matter absorption via electronic excitations*, JHEP **09** (2021) 123 [2106.12586].

149. A. Romanenko et al., *Search for Dark Photons with Superconducting Radio Frequency Cavities*, Phys. Rev. Lett. **130** (2023) 261801 [2301.11512].

150. M. Betz, F. Caspers, M. Gasior, M. Thumm and S.W. Rieger, *First results of the CERN Resonant Weakly Interacting sub-eV Particle Search (CROWS)*, Phys. Rev. D **88** (2013) 075014 [1310.8098].

151. S.R. Parker, J.G. Hartnett, R.G. Povey and M.E. Tobar, *Cryogenic resonant microwave cavity searches for hidden sector photons*, Phys. Rev. D **88** (2013) 112004 [1410.5244].

152. Z. Bogorad, A. Hook, Y. Kahn and Y. Soreq, *Probing Axionlike Particles and the Axiverse with Superconducting Radio-Frequency Cavities*, Phys. Rev. Lett. **123** (2019) 021801 [1902.01418].

153. H. Ueki and J.A. Sauls, *Photon Frequency Conversion in High-Q Superconducting Resonators: Axion Electrodynamics, QED & Nonlinear Meissner Radiation*, 2408.08275.

154. ALPS collaboration, *Towards the first axion search results of the Any Light Particle Search II experiment*, PoS **TAUP2023** (2024) 049 [2401.14773].

155. R. Janish, V. Narayan, S. Rajendran and P. Riggins, *Axion production and detection with superconducting RF cavities*, Phys. Rev. D **100** (2019) 015036 [1904.07245].

156. C. Gao and R. Harnik, *Axion searches with two superconducting radio-frequency cavities*, JHEP **07** (2021) 053 [2011.01350].

157. D. Salnikov, P. Satunin, D.V. Kirpichnikov and M. Fitkevich, *Examining axion-like particles with superconducting radio-frequency cavity*, JHEP **03** (2021) 143 [2011.12871].

158. CAST collaboration, *New CAST Limit on the Axion-Photon Interaction*, Nature Phys. **13** (2017) 584 [1705.02290].

159. CAST collaboration, *A new upper limit on the axion-photon coupling with an extended CAST run with a Xe-based Micromegas detector*, 2406.16840.

160. C. Vafa and E. Witten, *Parity Conservation in QCD*, Phys. Rev. Lett. **53** (1984) 535.

161. J.E. Moody and F. Wilczek, *NEW MACROSCOPIC FORCES?*, Phys. Rev. D **30** (1984) 130.

162. S. Bertolini, L. Di Luzio and F. Nesti, *Axion-mediated forces, CP violation and left-right interactions*, Phys. Rev. Lett. **126** (2021) 081801 [2006.12508].

163. L. Di Luzio, H. Gisbert, F. Nesti and P. Sørensen, *Axion Window on New Macroscopic Forces*, 2407.15928.

164. A. Arvanitaki and A.A. Geraci, *Resonantly Detecting Axion-Mediated Forces with Nuclear Magnetic Resonance*, Phys. Rev. Lett. **113** (2014) 161801 [1403.1290].

165. P. Agrawal, D.E. Kaplan, O. Kim, S. Rajendran and M. Reig, *Searching for axion forces with precision precession in storage rings*, *Phys. Rev. D* **108** (2023) 015017 [`2210.17547`].

166. P. Agrawal, N.R. Hutzler, D.E. Kaplan, S. Rajendran and M. Reig, *Searching for axion forces with spin precession in atoms and molecules*, *JHEP* **07** (2024) 133 [`2309.10023`].

167. ARIADNE collaboration, *Progress on the ARIADNE axion experiment*, *Springer Proc. Phys.* **211** (2018) 151 [`1710.05413`].

168. ARIADNE collaboration, *Source Mass Characterization in the ARIADNE Axion Experiment*, *Springer Proc. Phys.* **245** (2020) 71 [`2011.10141`].

169. D.A. Palken, *Enhancing the scan rate for axion dark matter: Quantum noise evasion and maximally informative analysis*, Ph.D. thesis, University of Colorado, 2020.

170. S. Chaudhuri, *Introducing the Princeton Axion Search (PXS)*, 2024 APS April Meeting, 2024.

171. J.L. Ouellet et al., *Design and implementation of the ABRACADABRA-10 cm axion dark matter search*, *Phys. Rev. D* **99** (2019) 052012 [`1901.10652`].

172. J.J.A. Baselmans, F. Facchin, A. Pascual Laguna, J. Bueno, D.J. Thoen, V. Murugesan et al., *Ultra-sensitive thz microwave kinetic inductance detectors for future space telescopes*, *Astronomy & Astrophysics* **665** (2022) A17.

173. P.K. Day, N.F. Cothard, C. Albert, L. Foote, E. Kane, B.H. Eom et al., *A 25-micrometer single-photon-sensitive kinetic inductance detector*, *Phys. Rev. X* **14** (2024) 041005.

174. C. O'Hare, "cajohare/axionlimits: Axionlimits." `https://cajohare.github.io/AxionLimits/`, July, 2020. 10.5281/zenodo.3932430.